Application and validation of Na/Ca as a proxy for seawater salinity in the Red Sea around Termination II

Jan Pieter Dirksen

First supervisor: Prof. dr. Gert-Jan Reichart
Second supervisor: Esmee Geerken

February 2016, Texel

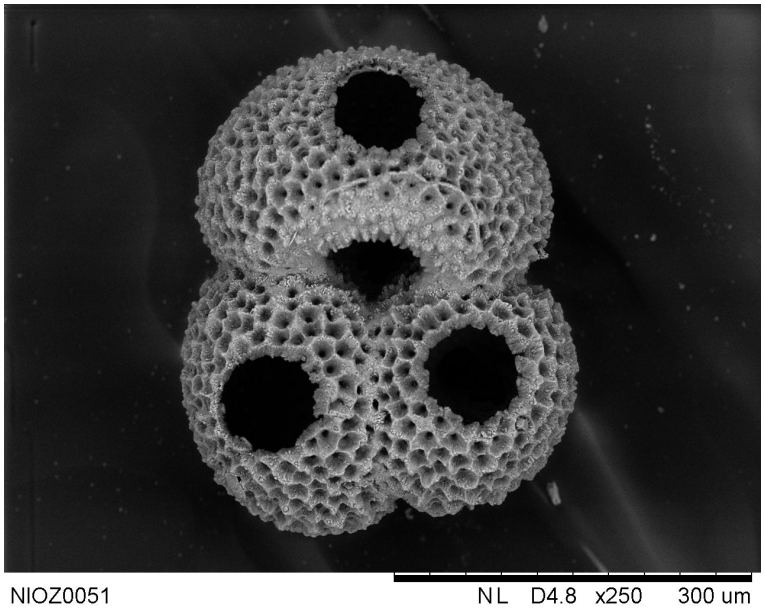

Figure 1: Scanning electron microscope image of a *Globogernoides ruber*, a common foraminifer used for paleoclimate reconstructions. Three holes have been ablated in the foraminifer for analyses

Abstract

In this study a novel approach to reconstruct salinity in the Red Sea on glacial-interglacial time scales is explored. This method combines Na/Ca, Mg/Ca and $\delta^{18}O_{Calcite}$ ratios measured on planktonic foraminifera. Samples from a piston core from the Red Sea (KL09) are used. Core tops from the Mediterranean Sea are used to compare Laser Ablation Inductively Coupled Mass Spectrometry (LA-ICP-MS) to solution Inductively Coupled Mass Spectrometry (solution ICP-MS). We find that solution ICP-MS can only be used effectively for Na/Ca and Mg/Ca when a sufficiently large sample group is used. For large amounts of samples with sufficient foraminifera, LA-ICP-MS requires significantly more time and solution ICP-MS is preferable. The results show that foraminiferal calcite Na/Ca from the sediment cannot be compared directly to plankton pump data, as this would result in unrealistic values for the calibration of the salinity proxy. We find that different species result in different Na/Ca values: the Na/Ca record of *Globogerinoides sacculifer* shows a similar trend with global sea level, while the record of *Globogerinoides ruber* (white) shows no correlation. The records are not of sufficient length for statistical significance, but promising for future research.

Contents

Chapter 1

Introduction

This research is part of the Netherlands Earth Science Center (NESSC, www.nessc.nl). The goal of the NESSC is to improve our understanding of the processes driving future climate change, and improve climate predictions and projections. Climate reconstructions are important for predictions and projections, as past conditions can give an analogy for the present. In this study, we aim to apply and validate a new, direct, sea water salinity proxy in the Red Sea, to improve the global sea level reconstruction (see section 1.5) and our understanding of past salinity. Salinity is a crucial component of the thermohaline circulation, and is directly related to sea level in the Red Sea (Siddall et al., 2004). Reconstructing past salinity may therefore provide information on changes in the thermohaline circulation in the future.

1.1 Orbital forcing and glacial cycles

When studying climate change in the geological past on glacial timescales, orbital forcing is one of the most important drivers (Hays et al., 1976). In this section we will explain how the orbital parameters affect global climate, and how this relates to our research. Insolation at a specific location and time (interval) depends on the position of the earth's orbit and rotational axis relative to the sun. This is described by the precessional motion and obliquity (tilt) of the rotational axis of the earth, and the eccentricity of the orbit of the earth. These variables change periodically, where each frequency depends on harmonic oscillations between the position, shape and orientation of the orbits of the planets (and to a lesser extent large asteroids) in our solar system. On timescales relative to our research (up to a few million years) this system is stable and chaos is not an issue. Therefore, if the present configuration of all relevant objects, as well as there masses are known, their positions can be calculated both for the future and the past (Laskar et al., 2011a). For paleoclimate reconstructions, this orbital solution is used to tune cyclic variations in lithology/proxy records to climate cycles, thereby interpreting variability in the tuned record as an expression of these cycles. Given that the phase relation and group delay (time delay of the amplitude envelope of each spectral component) are

known, this results in a highly accurate age model. Currently, a full astronomical solution is available for the past 54 Myr's, without further input (geological data), this is a definitive limit. For eccentricity, the short Lyapunov time of Ceres and Vesta (28.9 and 14.3 kyr) makes it impossible to extend the solution further back (Laskar et al., 2011b). Unpredictable variations in solar oblateness and tidal dissipation limit the calculation of precession and obliquity (Laskar, 1999). For the period in which we are interested (the last few 100 kyr's), global sea level is dominated by 100kyr eccentricity. This is an indirect effect, as the absolute change in insolation caused by this cycle is of insufficient amplitude to cause a deglaciation (Imbrie et al., 1992). However, the impact of eccentricity on the amplitude of climatic precession has a much bigger impact, and also affects seasonality (Zachos et al., 2001). This mechanism sets the boundary conditions for glacial cycles over the time period of interest.

In the marine isotope record, the expression of this cyclcity is used to divide the time scale in stages, known as Marine Isotope Stages (MIS). Currently, 104 MIS are defined, from 2.614 Ma (MIS 104), up to the present (MIS 1) (Lisiecki and Raymo, 2005). This research will focus on MIS6-5e, during which rapid changes in climate and sea level occurred as a response to the melting of the ice-sheets. Episodes of rapid climatic change during Earth's history are of special interest, as they help us understand the mechanisms and consequences of climate change in the present and near future. MIS5e is a good analogy for the future, as sea level rose to 6-9 meters above present sea level (De Boer et al., 2014), which is comparable to projection for the next 100 years. The melting of the ice sheets was triggered by insolation change (Grant et al., 2014), which was in turn driven by orbital forcing. Even though the current driver of climate change is an increase in greenhouse gas concentrations, not insolation change, the consequences may be similar.

1.2 Regional setting

In our research, we will focus on the Red Sea, located between the Arabian peninsula and Africa. The Red Sea is a young rift basin (Baker et al., 1996), with only a single natural connection to the open ocean in the South. The only natural passage to the open ocean is the very shallow Bab el Mandeb straight. As a result, sea level fluctuations associated with glacial cycles will directly affect the in- and outflow (Siddall et al., 2004). The circulation in the Red Sea is much more straightforward than in other semi-enclosed basins due to the geometry (see figure 1.1) (Siddall et al., 2004). Consequently, modeling paleo-climatic conditions is much less complex compared to, for example, the Mediterranean Sea. The samples we will study (taken from core GeoTü -KL09, 19' 57.60" N, 38' 08.30" E, see figure 1.1) are of Saalien-Eemien age, focussing on termination of the Saalien glacial (T2) and the start to the Eemian interglacial. The interval just before T2 is of greatest interest, as rapid changes in global climate and sea level are known to have occured

(Rohling et al., 2008). The termination itself cannot be studied in the Red Sea using foraminifera, as it is aplanktonic during this interval. The rapid change provides an analogy to the present and near future (the next 100 years)

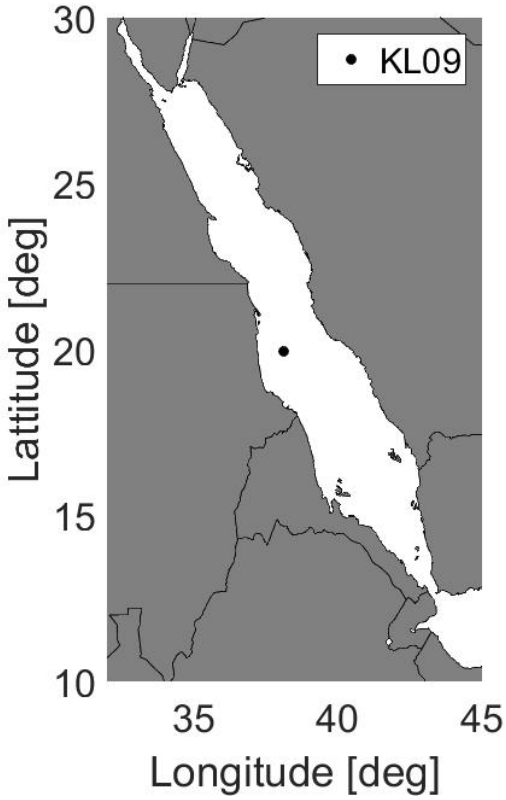

Figure 1.1: A map of the Red Sea showing the location of core KL09.

.

The core-top samples presented in this study originate from the Mediterranean Sea. A gradient in salinity is present between the sample sites. Like in the Red Sea, evaporation is higher than precipitation the Mediterranean Sea (Millot and Taupier-Letage, 2005). Inflow of less saline water mostly occurs at the straight of Gibraltar. Hence, salinity in the West of the Mediterranean Sea is lower than in the East (Millot and Taupier-Letage, 2005). This sample set is used to compare two different analytical methods: LA-ICP-MS and solution ICP-MS.

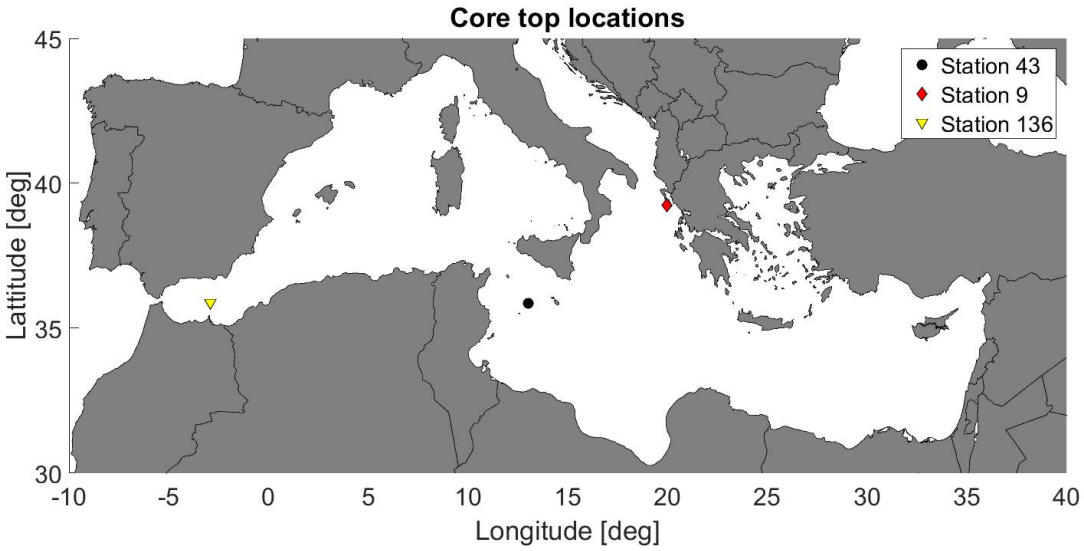

Figure 1.2: A map of the Mediterranean Sea showing the location of the core tops.
.

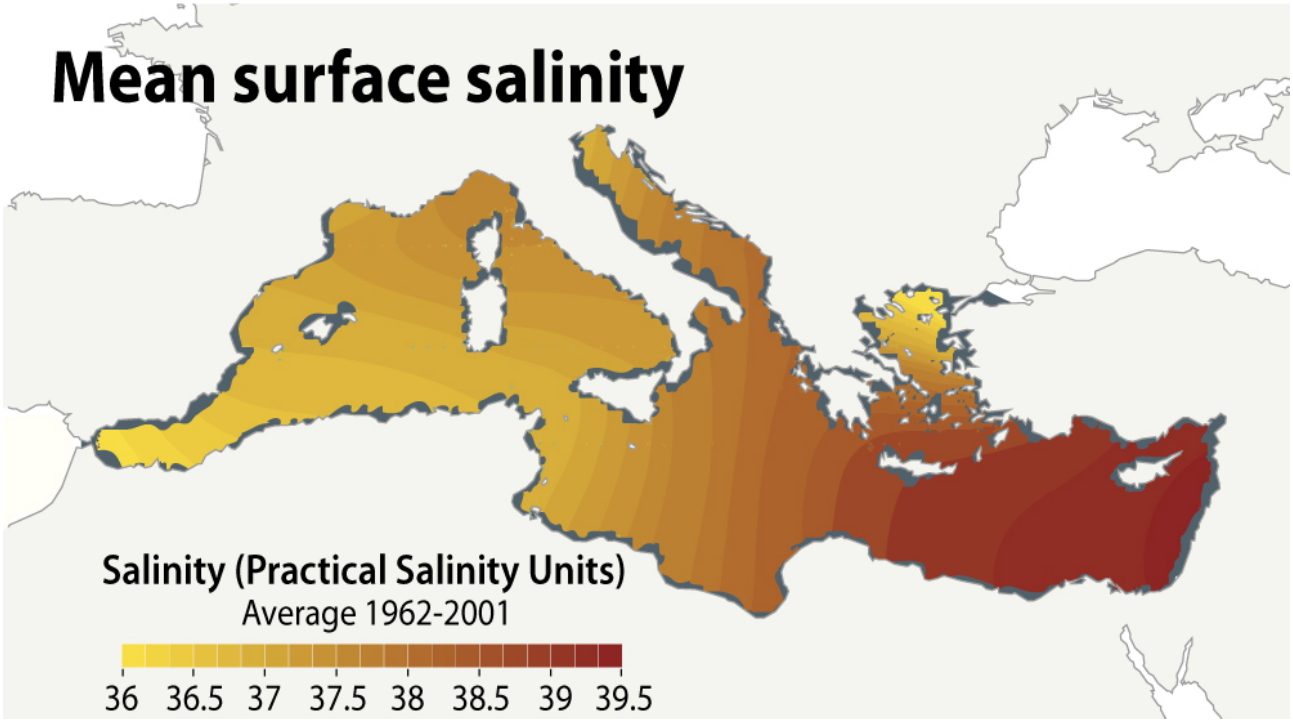

Figure 1.3: A map of the Mediterranean Sea showing the mean surface salinity. Adapted from Vidal et al. (2011). Note that salinity is higher in the east, and lower in the west.

1.3 Foraminifera

When studying paleoclimate, microfossils are an important tool. They are much more abundant than macrofossils, thereby providing greater statistical power and significance (Armstrong and Brasier, 2013). Their composition is determined by physiological processes and ambient conditions. The latter therefore partially reflects climate during the life of the organism. In this study we analyze the composition of two species of foraminifera to study paleoclimate. Foraminifera are single celled organisms that can both be found throughout the water column (planktonic) and at the water-sediment interface (benthic). The foraminifera we used (*Globigerinoides ruber* (*G. ruber*) and *Globigerinoides sacculifer* (*G. sacculifer*)) are both planktonic species that live in the mixed layer. *G. sacculifer* calcifies over a large depth range (0 to $> 314m$) (Rosenthal et al., 2000), while *G. ruber* calcifies closer to the surface (Wang, 2000). Therefore, any recorded paleoclimatic conditions reflect those at the depth at which the individual foraminifera calcified. Since the depth cannot be determined per individual, and temperature varies with depth, a direct relation between Mg/Ca in *G. sacculifer* cannot be established (Rosenthal et al., 2000).

1.4 Oxygen isotopes

When studying paleo-oceanography, oxygen isotopes are an important proxy for past climatic conditions. In this section, we will explain how this proxy works, and how it is applied.

The relative abundance of stable oxygen isotopes ^{18}O and ^{16}O in water is determined by several fractionation processes. In this chapter, we will explain the mechanisms controlling these processes and how we can use this information for paleoclimate reconstructions. Since both isotopes are stable, their total, global, amounts are constant through time. Two reservoirs of interest are the ice caps and glaciers combined (the global ice volume) and the oceans. When water evaporates, its $\delta^{18}O$ ratio will decrease, since ^{18}O is more dense then ^{16}O . Similarly, when part of the evaporated water precipitates, the $\delta^{18}O$ ratio of the remaining water will decrease further. This process is known as Raleigh distilation (for example Dansgaard (1964)). Since all ice on the polar ice caps is formed by evaporating water and transporting it over a significant distance, the ice has a very negative $\delta^{18}O$, which decreases with distance from the ocean. Consequently, as more water is stored in the cryosphere, the oceanic $\delta^{18}O$ will increase. Within the surface oceans, water evaporates at mid latitudes and rains out at the equator and high latitudes. Therefore, $\delta^{18}O$ is relatively high at mid latitudes, intermediate at the equator and low at high latitudes in the surface ocean.

The processes described above are the main factors determining $\delta^{18}O$ through space and time in the surface oceans. In this study, use a $\delta^{18}O$ record, established

by measuring foraminiferal shells (Rohling et al., 2008). During the formation of these shells, further fractionation occurs through different processes. While the exact physiological mechanisms are relatively unknown (and beyond the scope of this research), it is important to note that temperature, salinity and the species of the calcifier are important factors (Rohling et al., 2004).

The $\delta^{18}O$ levels found in a specific foraminiferal shell ($\delta^{18}O_{Calcite}$) will therefore reflect the ambient $\delta^{18}O$ (δw) and ambient conditions (mostly temperature and salinity). As we are interested in the global, temporal changes in sea level, we will need further information to solve this system. We will therefore also measure Na/Ca and Mg/Ca from the shells, as well as compare our data set to other data sets, such as the Antarctic $\delta^{18}O$ record.

1.5 Salinity reconstructions

Several proxies can be used for the reconstruction of past sea level and salinity. Residual $\delta^{18}O$ is widely used in the past, but has many pitfalls (Rohling and Bigg, 1998). Currently, most studies rely solely on $\delta^{18}O$ records for salinity reconstructions. However, this brings a number of insurmountable issues, resulting in a large inaccuracy (Rohling and Bigg, 1998): For an accurate reconstruction, the salinity:$\delta^{18}O$ relationship must be known at each point in time. However, due to spatial and temporal variations in sources, sinks and fluxes (such as freshwater budget or seasonal or permanent sea ice coverage) and the isotopic composition thereof, the salinity:$\delta^{18}O$ relation cannot be assumed to be linear or constant through both space and time (Rohling and Bigg, 1998). Alternatively, Na/Ca in calcite may be used (Wit et al., 2013). As salinity increases, the Na concentration in sea water increases. As new calcite precipitates, more Na will be incorporated. Foraminiferal Mg/Ca is a temperature proxy (Elderfield and Ganssen, 2000) ; with higher temperature, Mg/Ca will increase. In this study we will explore the combination of Na/Ca (Wit et al., 2013), Mg/Ca and $\delta^{18}O$ to decouple salinity, temperature and δw from the $\delta^{18}O_{Calcite}$ of foraminifera to achieve a more accurate salinity and sea level reconstruction. These results can be used to improve the sea level reconstruction model by comparing measured $\delta^{18}O_{Calcite}$ with modeled $\delta^{18}O_{Calcite}$ values. Furthermore, we will identify and attempt to solve issues inherent to the development of a new proxy.

Different species may show different responses to changes in environmental conditions. Biological control on Na incorporation appears to be present in at least some species (Wit et al., 2013), although it may be limited to differences in growth rate and size (which also affect Na/Ca of inorganic calcite). We will test this by measuring shell composition and size of two different species. Our aim is to identify the different parameters influencing Na/Ca and determine their magnitude. The establishment of a calibration to correct for these effects requires a culture study and is beyond the scope of this research.

1.6 Aim

In this study we aim to apply Na/Ca on a down-core record as a salinity proxy. The results of this method can be used to improve sea level reconstructions, as it can be combined with Mg/Ca to decouple temperature and salinity and δw in $\delta^{18}O_{Calcite}$, to reconstruct sea level This raises the following research questions:

• *Can foraminiferal Na/Ca be used as a salinity proxy in the Red Sea, to reconstruct sea level change during T2?*

• *Which analytical technique is most suitable for a down-core salinity reconstruction using foraminiferal Na/Ca? Should each foraminifera be analyze individually (Laser Ablation Inductively Coupled Mass Spectrometry (LA-ICP-MS)), or will whole sample analyses (solution Inductively Coupled Mass Spectrometry (solution ICP-MS)) give similar or better results?*

• *Is there a significant species and size effect on Na/Ca values?*

Chapter 2

Material & Methods

2.1 Material

To determine which analytical method is suited best for our research (see 2.2.1) we analyzed core tops from Mediterranean Sea samples and compared the results of two techniques: Solution ICP-MS and LA-ICP-MS. Our main goal, however, is to apply Na/Ca on a downcore record. To do so we studied samples from a Red Sea core (KL09), focusing on the Eemian-Saalien transition.

2.1.1 Mediterranean Sea core-top samples

From each of the three samples at least 25 *G. ruber* white and 5 *G. ruber* pink were picked. Additionally, from core 136, 25 G. *G. sacculifer* were picked and in each sample *G. ruber* white obliquus was seperated from the normal *G. ruber* white. The foraminifera have been cleaned following the Barker protocol (Barker et al., 2003), modified by Cambridge and NIOZ for the washing of the foraminifera for laser ablation ICP-MS. Next, each chamber in the last winding of each specimen has been measured using LA-ICP-MS. Afterwards, The *G. ruber* white (including *G. ruber* white obliquus) and G. *G. sacculifer* were curshed between two glass plates. The minimum distance between the plates was fixed by several layers of adhesive tape wrapped around the sides of one of the two plates to prevent over-crushing. The foraminifera were then cleaned a second time to remove material within the foraminifera for solution ICP-MS measurement.

Prior to the measurement of the Red Sea core samples, the standard error given an amount of measurements per data point has been calculated, see figure 3.2.

2.1.2 Red Sea core KL09

Samples of core KL09 are available through collaboration with the Australian National University in Canberra. From this core, 140 samples have been studied. Of these 140 samples, approximately 110 have been picked (the others contained

insufficient or no suitable foraminifera) and 40 have been analyzed for shell composition using either LA-ICP-MS or solution ICP-MS. Not all picked samples have been analyzed, as this was not feasible within the time constraints of this research (while picking all samples required minimal extra time). Two foraminifera species have been used for analyses: *G. sacculifer* and *G. ruber*.

The age model of Grant et al. (2014) has been used to determine which samples are to be analyzed and to compare our records to other climate reconstructions. Since direct age control is not yet possible in Red Sea sediments, an independent age model cannot be constructed. The age model of Grant et al. (2014) was established by comparing dust flux data of the Red Sea cores with the $\delta^{18}O$ record of the Sanbao cave in China (Cheng et al., 2012). This puts the samples in a broader perspective of global (climatic) conditions. Other researchers investigating KL09 (e.g. (Trommer et al., 2011)), published prior to Grant et al. (2014) use older age models, such as the one presented in (Rohling et al., 2008). It is therefore crucial to account for possible differences in dating, when comparing one data set to another. Each sample consists of $0.5cm$ of the core. From the age model, we can derive that each sample comprises 16 years. A higher resolution would result in insufficient foraminifera per sample and/or excessive noise.

2.2 Sample processing

2.2.1 Shell composition

In this study, the elemental composition of the shells of the foraminifera is investigated through two different techniques. Solution ICP-MS involves the dissolution of entire foraminifer tests and subsequent measurement of the composition of the dissolved material. Alternatively, a small amount of material may be ablated from individual foraminiferal shells using laser ablation. The ablated material is then measured in a mass spectrometer. LA-ICP-MS allows for the separate measurement of each chamber of every formaninifer, while solution ICP-MS always gives the average composition of all foraminifera in a sample. Although our study is focused on Na/Ca and Mg/Ca, we will also consider other elements as indicators for several factors, such as contamination (see subsection 3.2.1).

2.2.2 Sample preparation

First, the samples were washed through seives to isolate the relevant fraction. Then, we picked two foraminifera species: *G. ruber* (*G. ruber* and *G. sacculifer* (*G. sacculifer*). Of each species, at least 25 individuals have been picked per sample. In some samples, there where insufficient foraminifera of one or both of the relevant species. In these cases, either all acceptable specimens where picked to be analyzed, or the sample was rejected. Samples to be analyzed with solution ICP-MS were weighed prior to crushing to confirm that sufficient material was present in each sample. Next, the forams have been cleaned following the Barker protocol

(Barker et al., 2003) modified by Cambridge and NIOZ. First, clay and coccoliths are removed by utrasonicating and agitating each sample with milli Q and removing the supernatant after settling of the coarse material. This step is repeated 4 times and an additional 2 times with methanol instead of milli Q. Next, organic matter is removed by adding NH_4OH buffered H_2O_2 (although the cambridge protocol uses NaOH, we used NH_4OH for the removal of organic matter, as the high Na concentrations in NaOH could influence Na/Ca ratios of the foraminiferal calcite) to each sample, placing the sample rack in a 95^o and ultrasonicating the samples afterwards. This step is repeated twice, after which any remaining oxidizing reagent is removed by filling each sample tube with milli Q and removing the supernatant after settling (repeated at least three times) For LA-ICP-MS, this is the final step of the cleaning protocol, allowing the foraminifera in each sample to be placed on a stub, with the final winding facing up.
For solution ICP-MS, absorbed ions have to be removed. To do so, each sample is first transferred to a new, leached, tube. Then, dilute acid leach (0.001M HNO_3) is added to each sample. The samples are then ultrasonicated for 30 seconds, removing the acid directly thereafter. To remove any remaining acid, ultrapure water is added to the tubes and removed after settling of the material (repeated once).

2.3 ICP-MS Protocols

Both sets of foraminifera (Mediterranean Sea core tops and Red Sea core KL09) were ablated with a NWR19UC (New Wave), that uses a ArF excimer laser with $193nm$ pulse width. The laser was set at a repetition rate of 6Hz and an energy density of $1(\pm 0.05)J/cm^2$. Each chamber in the final winding of each foraminifer was ablated in a New Wave TV2 cell during 60 seconds with a round spot with an $80\mu m$ diameter. A short wash-out using a 30 second warm-up of the laser and 30 second wash-out to remove the aerosol out of the cell and tubing was used. Helium (with a flow rate of $0.7l/min$) was used to transport the aerosol of small particles to a quadrupole ICPMS (Thermo Scientific iCAP$-$Q) using a smoother for increased stability. To obtain stable plasma and increase sensitivity, $0.3l/min$ nebulizer argon gas and $5ml/min$ nitrogen was mixed with the helium flow. The nebulizer argon gas, extraction lens, CCT focus lens and torch position were daily autotuned for the highest sensitivity of 24Mg and low ThO/Th ratios ($< 1\%$) ablating a synthetic $CaCO_3$ standard (MACS3) using a line-scan pattern. These tuned parameters are summarized in Table 2.3.

2.3.1 HR-ICPMS

Trace elements were measured by an intensity ratio calibration method on a HR-ICP-MS (ThermoFinnegan, Element-2). Approximately $0.3mg$ of crushed foraminifera was cleaned following the method of Barker et al. (2003). After cleaning, the sample was dissolved in a $0.5ml$ ultraclean $0.1M$ HNO_3 acid. For pre-analyses of the

N_2	5
CCT Entry Lens (V)	-103
Cool Flow (l/min)	14
Sampling Depth (mm)	3
Plasma Power (W)	1150
Auxilliary Flow (l/min)	0.80
Nebulizer Flow (l/min)	30
Torch Horizontal Position	-0.7
Torch Vertical Position	1.5
Extraction Lens 2 (V)	-93

Table 2.1: Tune settings

calcium content, a subsample of $0.030ml$ was diluted 10 times. Directly before analyses all samples and standards were diluted to a constant $20 \pm 5ppm$ calcium matrix to avoid matrix corrections. For optimal precision and accuracy elements were measured in 3 resolutions: ^{25}Mg and ^{23}Na was measured in low resolution, ^{27}Al, ^{55}Mn and ^{56}Fe in medium resolution and ^{39}K in high resolution (interference of ^{38}Ar^{1}H). The internal standard ^{43}Ca was measured in all resolutions. Details of the acquisition method are listed in table 2.3.1.

Analyses time (min)	3
Uptake time (s)	80
Rinse time (s)	10
Sample time LR (ms)	0.01
Sample time MR (ms)	0.02
Sample time HR (ms)	0.03

Table 2.2: Acquisition Method

The instrument sensitivity was optimized daily using a Finnegan tune solution and a foraminifera solution with added cerium to monitor oxides. To obtain a stable signal and low detection limit, a dual spray chamber in combination with the components listed in 2.3.1 was used

Uptake	Pumping
Sample introduction	Cross flow nebulizer
Cooling	Peltier
Nebulizer flow rate	$300\mu l/min$
Spray chamber	Dual
Sample cone	Aluminium
Skimmer cone	Aluminium

Table 2.3: Instrument configuration

Drift was corrected using linear interpolation between two monitor standards. After each 5^{th} sample a drift and monitor standard was measured. Drift correction was applied in a R-script using the Loess function (local polynomial regression fitting).

2.4 Data analyses

The LA-ICP-MS data has been integrated in Qtegra. Blank intervals were maximized for optimal significance. Initial peaks (at the surface of the test), have been excluded from analyses (see figure 2.1). Intervals showing a-typical composition in one or more elements (most notably calcium) were not integrated. Next the elemental concentrations were exported to excel. In excel, elemental ratios were calculated and foraminiferal species, chamber and age were added to each data point. If necessary, outliers were removed (see subsection 3.2.1). Solution ICP-MS data was acquired as an excel file, only ratios had to be calculated and ages per sample added. All further analyses and plotting has been conducted in Matlab (R2015b) (see Appendix B). Data sets have been organized in subsets per sample, chamber, species and combinations thereof. Finally, all relevant plots were made, including time series and XY plots. Interpolations were achieved using the matlab curve fitting toolbox. All maps (figures 1.2 and 1.1) were constructed using a matlab script (see appedix B.3) and 'Natural earth' shapefiles (available from naturalearthdata.com) for border locations.

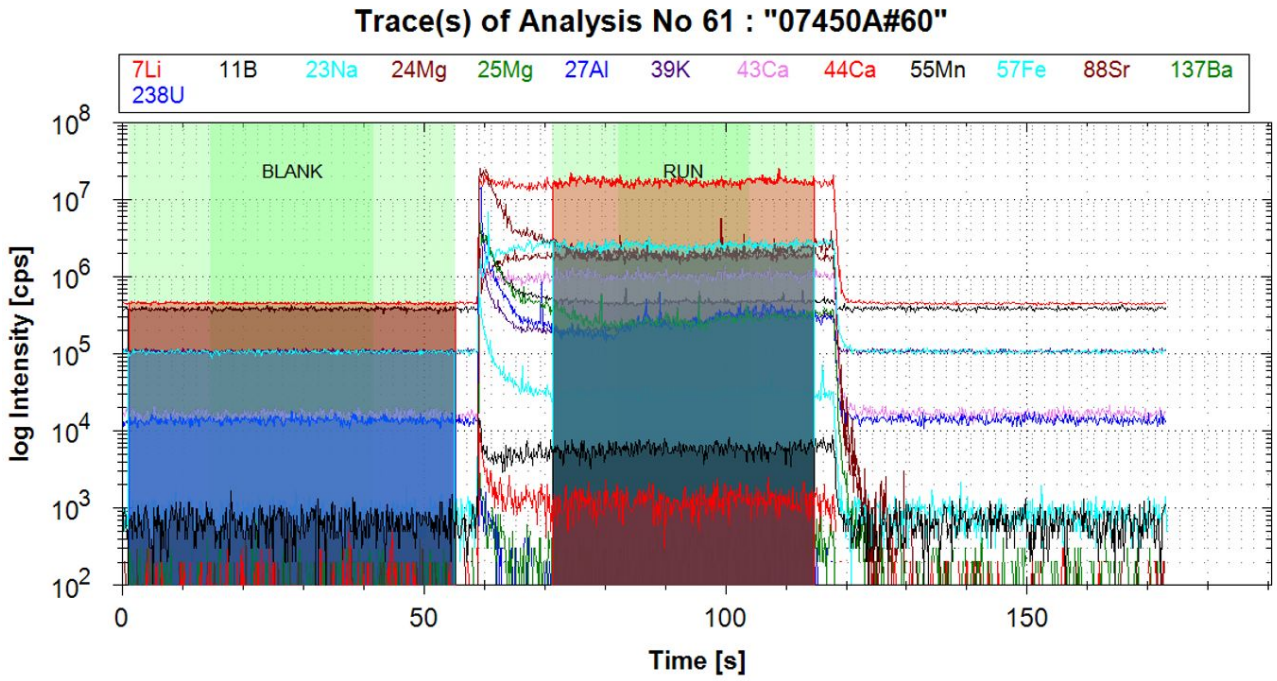

Figure 2.1: An ablation profile of the F-2 chamber of a foraminifer. Note that initial peaks in elemental concentrations are excluded from the integration.

Chapter 3

Results

3.1 Core-top samples

The core-top samples originate from three different location in the Mediterranean Sea (see figure 1.2), each with a different salinity (figure 1.3). When compared to the Red Sea calibration curve (plankton pump data, sea figure 3.1, in prep.), the Na/Ca ratios of our measurements

Although a trend is present, standard error is relatively large (see figure 3.1). *G. ruber* (pink) is not shown, as only five individuals (15 spots) have been measured per core-top of this sub-species. This is considered to be non-representative, as the expected standard error for 15 measurements is too high (see figure 3.2. The Red Sea plankton pump data)

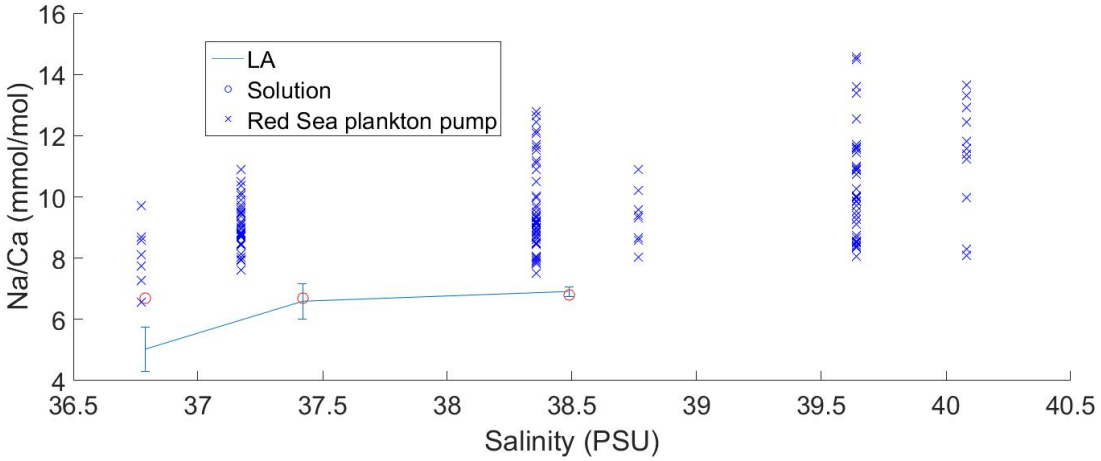

Figure 3.1: Errorbar and scatter plot showing Na/Ca of *G. ruber* over the measured range of salinity, circles indicate solution ICP-MS measurements, crosses indicate Red Sea plankton pump data (in prep.). This is the main result of this section. Errorbars indicate standard error.

LA-ICP-MS and solution ICP-MS measurements have both been performed on the same samples for comparison of the two methods (see figure 3.1). We found that two out of three core tops gave the same Na/Ca for both methods, while one gave a higher Na/Ca with LA-ICP-MS, although still within the standard deviation.

The LA-ICP-MS data also shows that there is no significant difference between *G. ruber* (white) and *G. ruber* obliquus (white). *G. ruber* (pink) appears to have different Na/Ca ratios compared to *G. ruber* (white) at each core-site (see figure 3.3). However, insufficient *G. ruber* (pink) have been analyzed for a definitive conclusion. These results are in line with expectations, as *G. ruber* (white) and *G. ruber* obliquus (white) are of the same species and *G. ruber* (pink) is not.

Prior to the analyses of the Red Sea core samples, standard error (1σ) in Na/Ca per sample was calculated for the Mediterranean Sea core tops as a function of the amount of spot measurements (figure 3.2). This allows us to estimate how many measurements per sample are required for a representative sample group. We find that 90 measurements per sample gives an acceptable standard error, without requiring excessively large amounts of foraminifera.

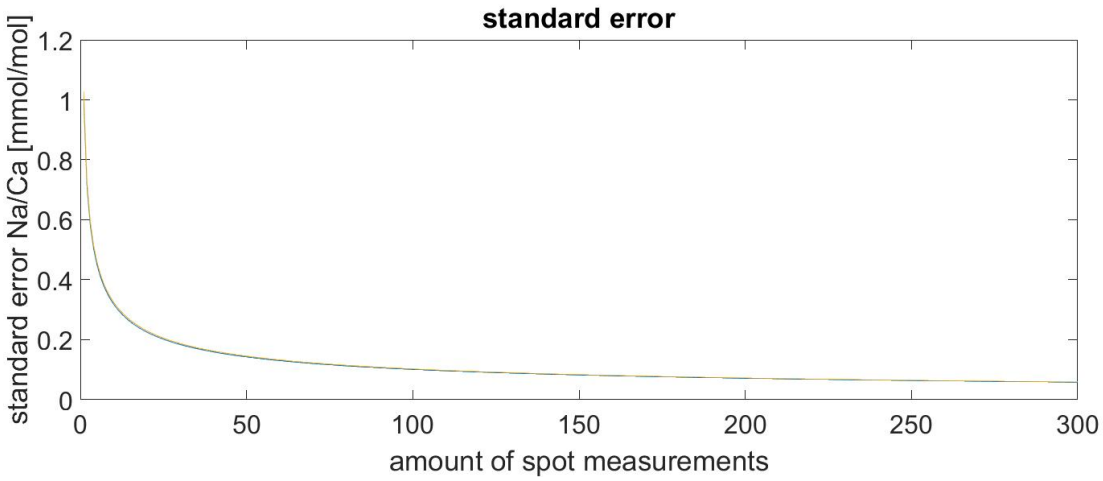

Figure 3.2: Standard error (1σ) in Na/Ca, for all measurements of each core-top. About 90 measurements result in an acceptable standard error of about 0.1 mmol/mol. This equates to 30 foraminifera (three measurements per chamber, therefore we picked 30 foraminifera per sample from Red Sea core KL09.)

Since each chamber is measured individually with LA-ICP-MS, intra-individual variability can be assessed (see figure 3.3). In each core, the first two chambers of the final winding of *G. ruber* (white) (F-1 and F-2) a large spread, with a similar mean(see figure 3.3). The final chamber (F) shows a the same average,but a much smaller standard error, compared to the other chambers. For *G. ruber* (pink), only 5 foraminifera have been measured per core top sample, giving a non-representative data set.

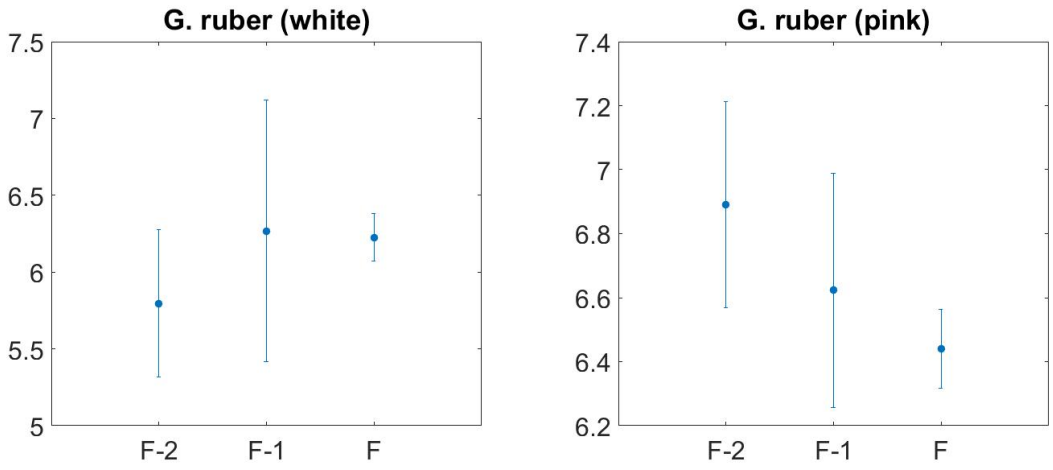

Figure 3.3: Here, errorbar plots of Na/Ca are given for all core-tops, per chamber of all foraminifera measured from the core top samples. The errorbars indicate standard error (1σ).

3.2 Red Sea core samples

Core KL09 originates from the middle of the Red Sea (see figure 1.1). The samples just before T2 contain some foraminifera, albeit very little. Hence, there is not enough material to study these samples at highest resolution with solution ICP-MS. Therefore, these samples are studied with the LA-ICP-MS. The interval after T2 contains abundant foraminifera (both *G. ruber* (white) and *G. sacculifer*). Studying all of these samples with the LA-ICP-MS is not feasable within the time constraits. The samples are therefore measured using solution ICP-MS. The size (see figure 3.4)) of each foraminifer has been measured to study a possible effect on shell composition (see figures in (Wit et al., 2013) and figure 3.6). Since our core top samples showed little intra-individual variability (figure 3.3), we decided to measure only the full size of the foraminifera instead of each individual chamber.

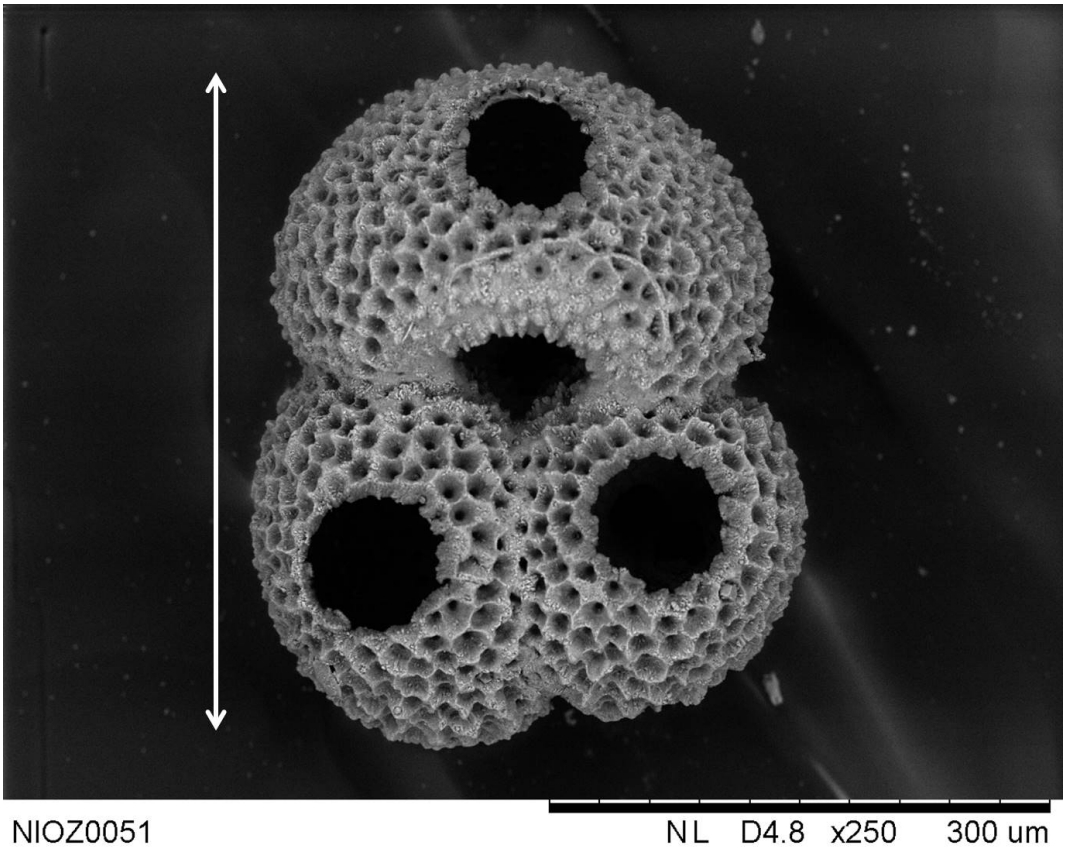

Figure 3.4: A scanning electron microscope picture of *G. ruber*. The size of the foraminifer is indicated by the white arrow. A hole was ablated in each of the three chambers in the final winding for LA-ICP-MS measurement.

3.2.1 Data filtering

All unrealistic ratios ($> 1000\ mmol/mol$ or negative concentrations) were excluded from further analyses. For LA-ICP-MS, absolute Mn/Ca and Fe/Ca values are not reliable due to interference with other elements. For example, N and Ar isotopes (both used for LA-ICP-MS measurements) have the same combined mass as Fe. Although these isotopes comprise a only a small fraction of the gasses, the large amount of gas used causes them to significantly influence the measurements of Mn and Fe. This results in a high threshold, with actual variability superimposed. However, trends can still be used to identify outliers. Very high Mg/Ca ratios have been found in the Red Sea data (see figures A.1 up to A.5). This may be caused by contamination or overgrowth of non-biogenic calcite (Hoogakker et al., 2009). If this is the case, a correlation between high Mg/Ca and high ratios of the other elements is expected. Note that the solution ICP-MS data points are averages of a sample; even if the average ratio of an element is below the upper limit, in-

dividual foraminifera may still have been contaminated. To exclude such outliers from further analyses, Mg/Ca has been plotted against elements which are commonly associated with contamination (see figures A.1 up to A.5) (Ferguson et al., 2008).

Method	Fe/Ca	Al/Ca	Mn/Ca	Li/Ca	Mg/Ca	Na/Ca
LA	$1 * *$	2	$0.4 * *$	-	35	10
Solution	$*$	-	0.15	$*$	35	10

Table 3.1: Upper limits for KL09 data $[mmol/mol]$

$*$: Not measured; $**$: Absolute values not reliable due to interference with other elements; -: All ratios were found to be below conventional ratios (Ferguson et al. 2008).

XY plots (see figures A.1 up to A.5) are given for elements associated with contamination versus Mg/Ca. solid lines in each plot indicate the upper limits per element ,also given in table 3.2.1. Data points above an upper limit are excluded from further analyses. Note that limits for Na/Ca and Mg/Ca are arbitrary: All data points with higher Na/Ca or Mg/Ca are also rejected for at least one other element being too high. In this way, contaminated samples are rejected without relying on their Na/Ca or Mg/Ca.

3.2.2 Distributions and XY-plots after filtering

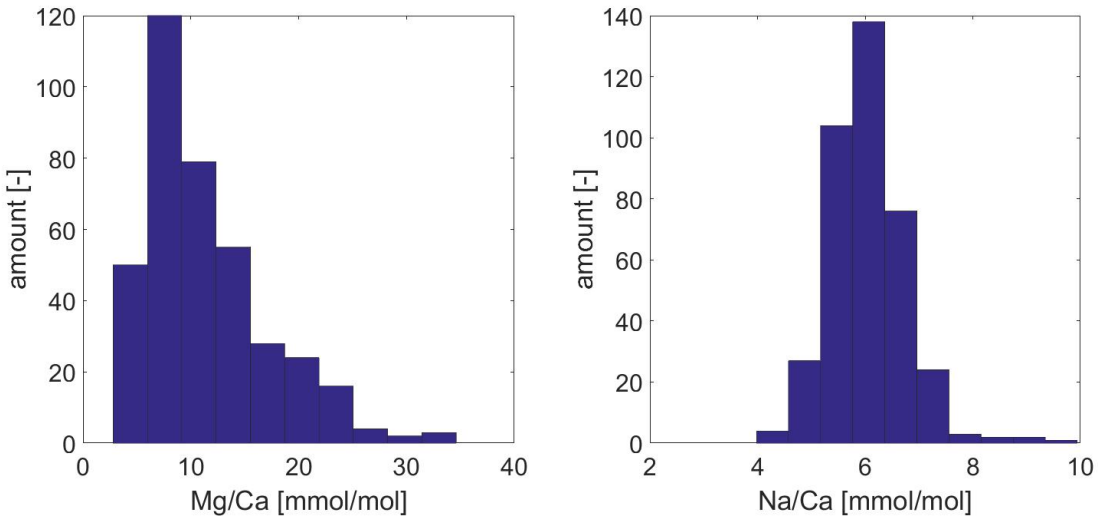

Figure 3.5: Two Histograms showing the distribution of all LA measurements from core KL09 after filtering, with Mg/Ca on the left and Na/Ca on the right. No trends are found.

The historgram (figure 3.5) shows that Mg/Ca is not normally distributed, with a tendency towards higher ratios. Na/Ca shows an almost perfect normal distribution, with very few outliers. Although the outlier removal (see section 3.2.1) inherently alters the distribution, it is important to note that all removed data points had too high concentrations of at least one ratio other than Na/Ca or Mg/Ca (see table 3.2.1). Therefore, it is not trivial that removing outliers will result in a specific distribution.

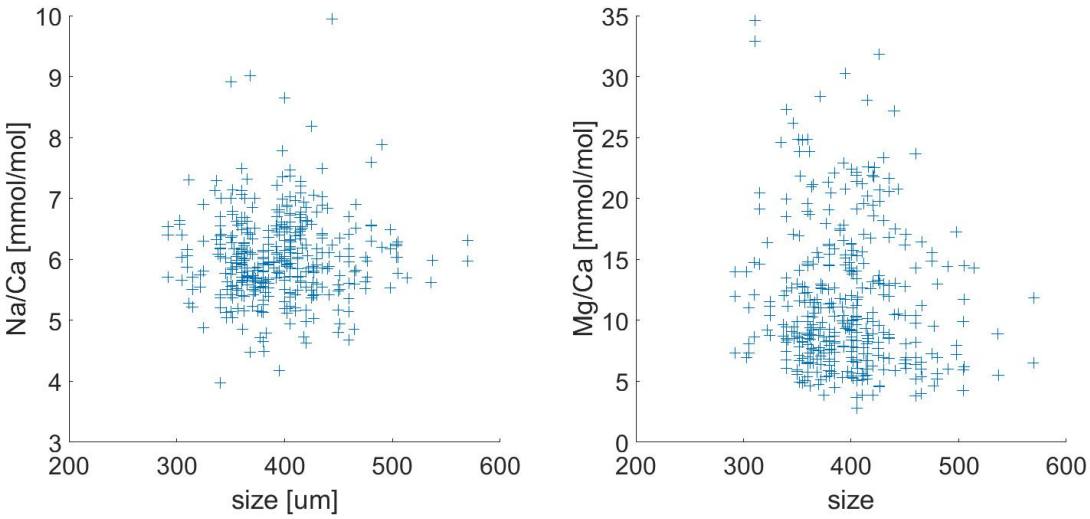

Figure 3.6: Two XY-plots showing size versus Na/Ca and Mg/Ca.

Size has been measured of each foraminifer from core KL09 analyzed with LA-ICP-MS. The results can be seen in figure 3.6. No significant correlation has been found between size and Mg/Ca as well as Na/Ca.

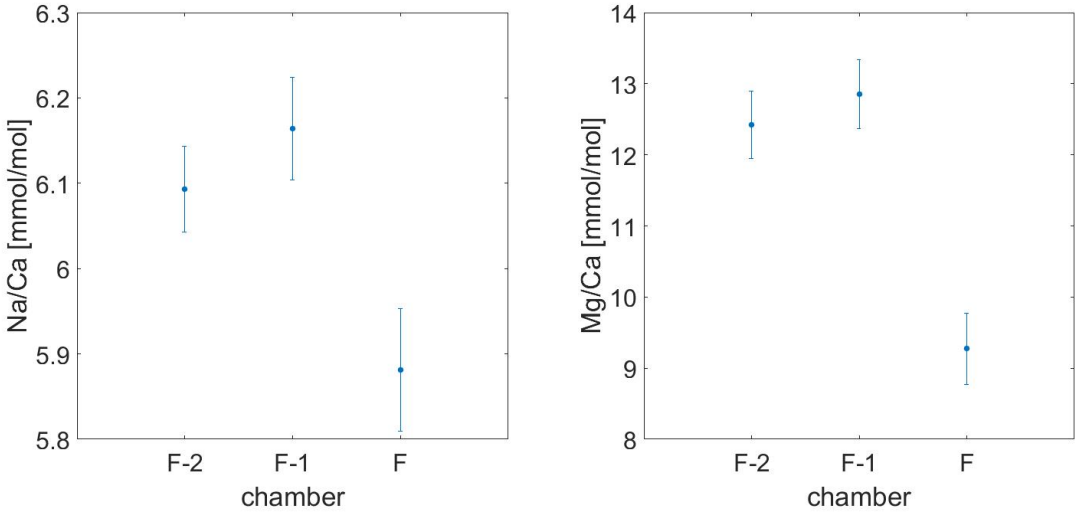

Figure 3.7: Two error-bar plots showing chamber versus Na/Ca (left) and Mg/Ca (right). The error-bars indicate standard error (1σ)

Figure 3.7 shows the relation between chamber and both Na/Ca and Mg/Ca. Note that Na/Ca as well as Mg/Ca is found to be lower in the final chamber. Differences in Na/Ca as well as Mg/Ca between the first two chamber (F-2 and F-1) are found to be within the standard error.

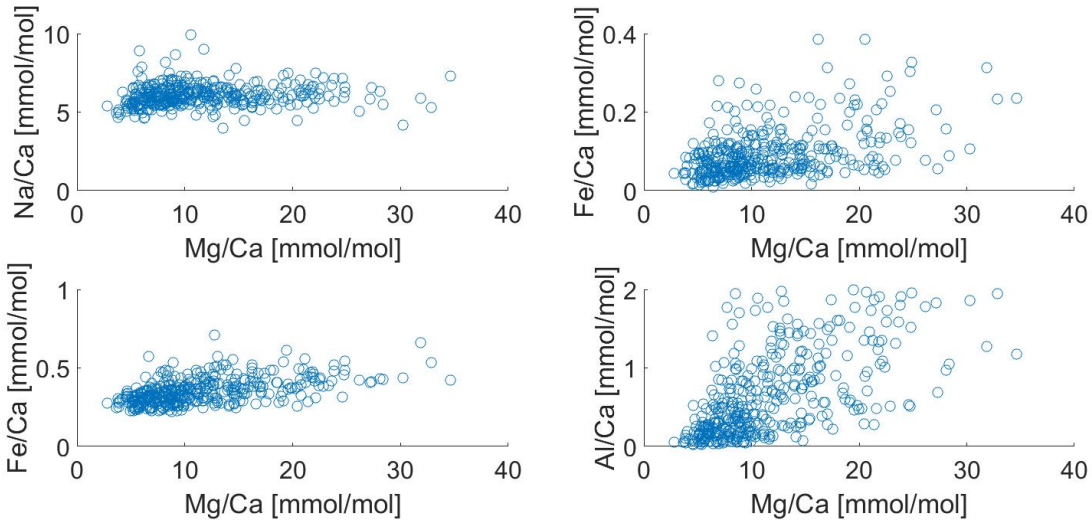

Figure 3.8: XY-plots after filtering

Prior to filtering, a clear corrrelation between high Al/Ca and high Mg/Ca has been found (see figures in appendix A). After filtering , all data points with

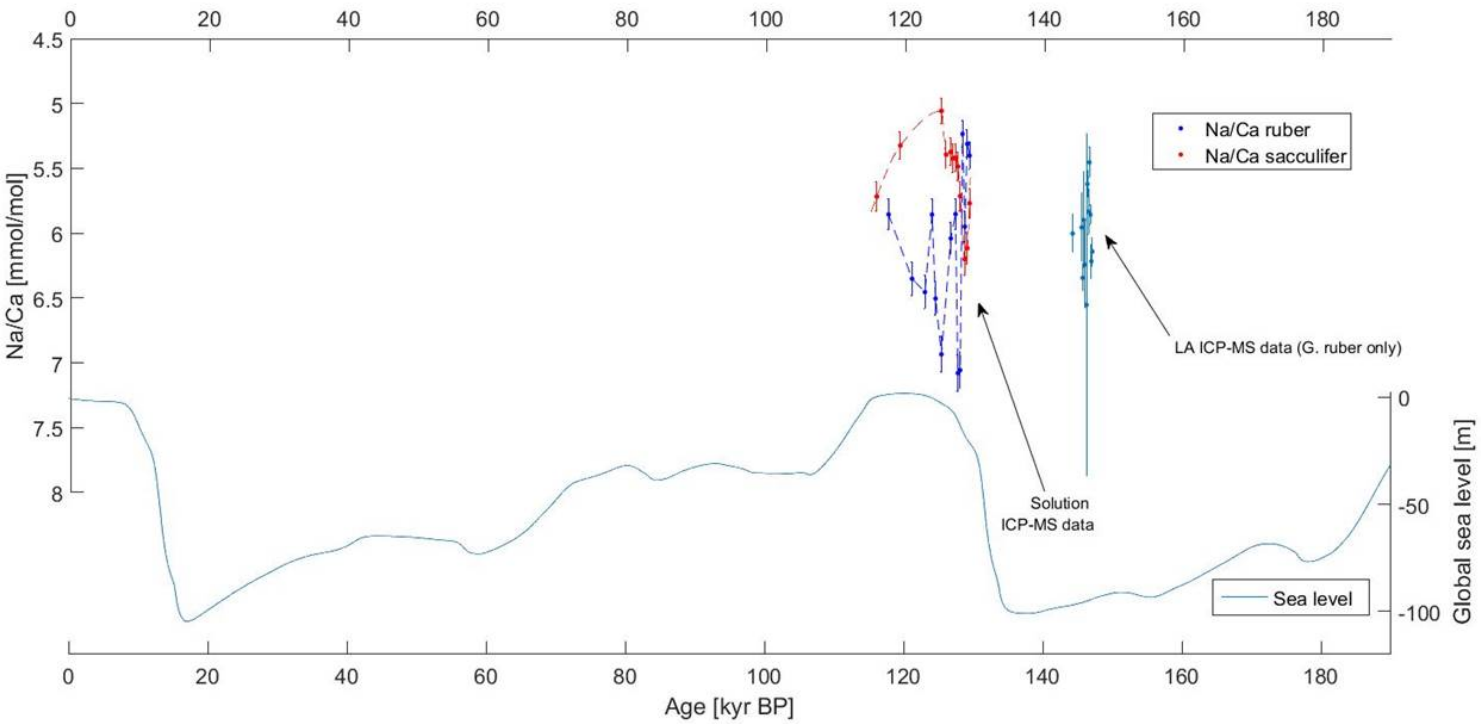

Figure 3.9: The solid line represents global sea level (De Boer et al., 2014), compared to the Na/Ca record of KL09 (obtained from both *G. ruber* and *G. sacculifer*, dashed line and individual data points). Error bars show measurement error only for solution ICP-MS and standard error (1σ) for LA-ICP-MS. Age model (for the Na/Ca and Mg/Ca records) from Grant et al. (2014), Global sea level from (De Boer et al., 2014).

Na/Ca>10 and Mg/Ca>35 are excluded and the trends are no longer present (figure 3.8).

3.2.3 Trends in sea level compared to Na/Ca and Mg/Ca

Here we will put our data in a broader perspective by comparing Na/Ca and Mg/Ca to a global sea level reconstruction (De Boer et al., 2014) (figures 3.11, 3.10 and 3.9). The core extends from $150kyr$ up to $30kyr$, on average 1 sample ($0.5mm$) therefore represents 16 years. Figure 3.9 shows an overview, while figure 3.10 shows a detailed view of the time period of our data sets. Note that Na/Ca of *G. sacculifer* shows a similar trend as sea level, while the record of *G. ruber* does not. The Mg/Ca record shows a similair trend, compared to sea level (see figure 3.11).

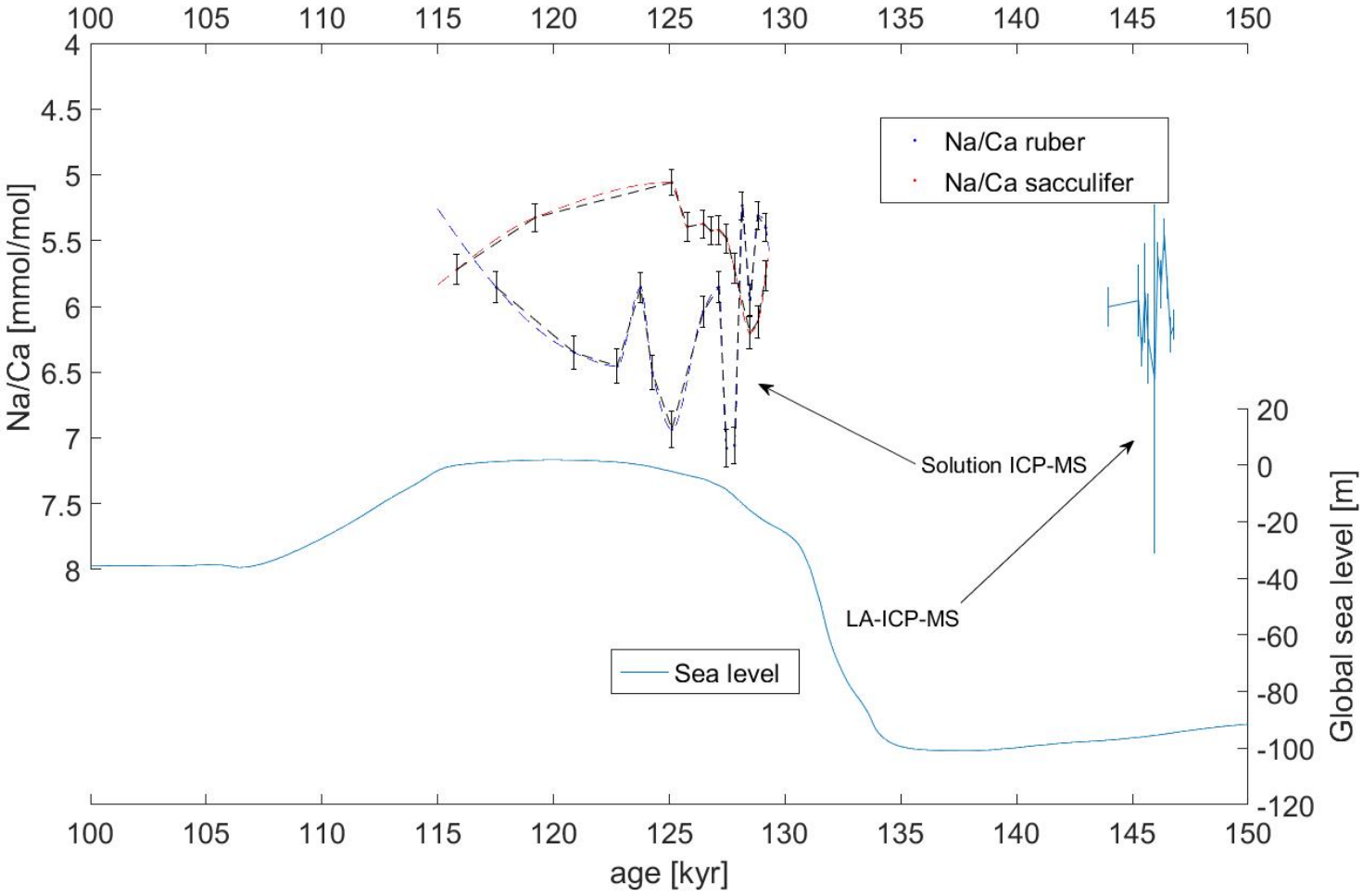

Figure 3.10: A zoom in of figure 3.9, this is the main result of this section. The solid line represents global sea level (De Boer et al., 2014), compared to the Na/Ca record of KL09 (obtained from both *G. ruber* and *G. sacculifer*). Error bars show measurement error only for solution ICP-MS and standard error (1σ) for LA-ICP-MS. Age model from Grant et al. (2014), Global sea level from De Boer et al. (2014).

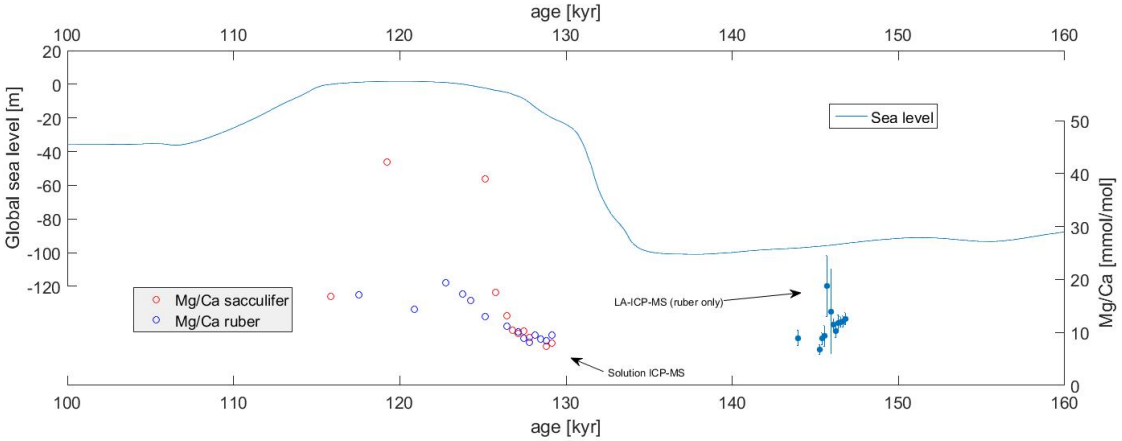

Figure 3.11: A comparison between sea level (solid line) (De Boer et al., 2014) and Mg/Ca.

Chapter 4

Discussion

4.1 Solution-ICP-MS versus LA-ICP-MS

We used both Solution ICP-MS and LA-ICP-MS to analyze foraminiferal shell composition. In this section we will discuss the differences between the methods. Solution ICP-MS requires more labwork: acid leaching, dissolution and dilution of the samples. For LA-ICP-MS however, targets need to be set for each spot to be measured (foraminifera and standards). For small quantities of samples and/or foraminifera, LA-ICP-MS is more time efficient, while for larger sample sets, Solution ICP-MS takes less time. One of the core top samples gave a higher Na/Ca with LA-ICP-MS than with solution ICP-MS. Since this core top originates from a location with lower salinity, lower Na/Ca is expected. The LA-ICP-MS data shows this, while the solution ICP-MS data does not.

When compared to the Red Sea calibration curve (in prep., see figure 3.1), Na/Ca in the core tops used in this study is found to be lower, although the trend with salinity is similar. The difference in Na/Ca could be the result of a difference between plankton pump and core top data. Alternatively, the salinity used for the core top data may not be the salinity at which the calcite formed.

Solution ICP-MS returns a single data point for the whole sample, while LA-ICP-MS gives data per spot measured. For paleoclimate reconstructions, we are interested in a time-series, therefore a single data point per sample would be sufficient. However, if any of the foraminifera are contaminated or diagenetically altered, a solution ICP-MS measurement of the sample would return non-representative values. With LA-ICP-MS, outliers in terms of shell composition can be removed, eliminating the issue to a certain extent (if all foraminifera are contaminated, individual measurements will not help either). Especially in high salinity environments, such as the Red Sea, non-biogenic calcite overgrowth is to be expected (Hoogakker et al., 2009). Such overgrowth can have very high Mg/Ca ratios (Hoogakker et al., 2009), resulting in measurements comparable to our data set. If overgrowth is present on our samples, laser ablation profiles should show a high

peak in Mg/Ca on the outer layer of the foraminifera and normal values further down the test. However, for all LA-ICP-MS measurements, all innitial peaks were excluded from integration (see figure 2.1). It is therefore likely that another process is causing atypical Mg/Ca ratios. Moreover, a histogram of all Red Sea LA measurements (figure 3.5) shows that relatively few data points are far from a normal distribution. Na/Ca in these measurements does not show many outliers (figure 3.5). However, unlike Mg/Ca, non-biogenic Na/Ca is not much higher or lower than biogenic Na/Ca. It is therefore unlikely that the Na/Ca record is dominated by overgrowth. Again, it is important to use LA-ICP-MS, as with solution ICP-MS alone, outliers cannot be detected and removed. Note that even contaminated foraminifera could result in a normal distribution in Mg/Ca and Na/Ca.

The cleaning protocol for LA-ICP-MS limited the amount of foraminifera per $0.5ml$ tube to 10. The reasoning being that ultrasonication would otherwise cause foraminifera to hit each other too hard, causing fracturing. However, a revision of the ultrasonic bath settings (lower power, higher frequency), removed this limitation. As a result, only one $0.5ml$ tube is needed per sample, shortening the time needed by a factor of 3 (considering samples contain 25-30 foraminifera).

4.2 Red Sea core samples

4.2.1 Data quality

The coretop samples show that differences in salinity smaller than 1 psu may not be observable in Na/Ca records, unless a large amount of individuals is measured. A standard error analyses (see figure 3.2) shows that with current techniques, a standard error of $<$0.1 mmol/mol Na/Ca is not feasible, as hundreds of foraminifera would be needed per sample. In some samples, mostly those just below T2, insufficient foraminifera where present for a reasonable standard error in Na/Ca. Furthermore, a large amount of the foraminifera in this interval could not be used for further analyses, as their composition indicated overgrowth or contamination (see figures A.1 up to A.5 and section 3.2.1). The temporal resolution should therefore be sufficiently high, aliasing is not a problem. Bioturbation and other diagenetic processes may have acted as a low pass filter through mixing of sediment. However, this would only cause a reduction in high frequency variability, without generating a large group delay. Both Na/Ca and Mg/Ca show a distinctly different ratio in the final chamber, compared to the F-1 and F-2 chambers (see figure 3.3) in the KL09 LA-ICP-MS data set (only *G. ruber*). If this was caused by contamination, the opposite would be expected, as the final chamber is much thinner than the F-1 and F-2 chambers and inorganic Mg/Ca is typically higher than organic Mg/Ca in foraminifera (Hoogakker et al., 2009). Therefore, the same amount (by mass) of contamination would have a larger impact on the Na/Ca and Mg/Ca ratios. The observed intra-individual variability could be an ontogenic effect, in which case it is not clear which of the chambers are atypical, and should be excluded from

analyses. We therefore decided to included all chambers in the rest of this study.

4.2.2 Inter-species variability

The Na/Ca record of core KL09 is different for each of the species analyzed (see figure 3.10). Possibly, this is related to the different habitats in which the species live: *G. ruber* lives at the surface (Armstrong and Brasier, 2013), while *G. sacculifer* calcify over a very large depth range (Rosenthal et al., 2000). Differences in growing season may also influence the records. The composition of each chamber and test therefore reflects paleoclimatic conditions of different depths. Therefore, it is to be expected that the Mg/Ca records of *G. sacculifer* and *G. ruber* are different. However, for the interval were both species are analyzed, trends in Mg/Ca are comparable, disregarding two outliers in the record of *G. sacculifer* (see figure 3.11). This could suggest that differences between the habitats of each species were small, that measuring >25 individuals per sample evens out any differences, or that the samples are contaminated. Alternatively, the gradient in temperature over the depth range at which *G. sacculifer* may not be sufficient to cause a shift in Mg/Ca above the detection limit (compared to the surface), or all analyzed *G. sacculifer* may have calcified most of their test at the surface. With the current data-set , it is not possible to distinguish between these options.

4.2.3 Trends in Na/Ca and sea level

At the start of the interglacial, sea level rose considerably (Trommer et al., 2011; De Boer et al., 2014) (also see figure 3.10). Consequently, it is expected that the increase in area through which water can flow into the Red Sea will cause salinity to decrease (see section 1.2). When compared to a global sea level reconstruction (De Boer et al., 2014), *G. sacculifer* shows a similair trend in Na/Ca and Mg/Ca (see figures 3.11and 3.10). However, the interval over which *G. sacculifer* has been analyzed is very short. Further analyses is therefore needed to strengthen this result. Na/Ca in *G. ruber*, however shows no correlation with sea level. If a correlation between Na/Ca in *G. ruber* would exist, higher Na/Ca would be expected in the samples below T2, when sea level was lower (see figure 3.10), which is not the case. While contamination might explain the measurements on the samples below T2, the same reasoning can not explain the differences between *G. sacculifer* and *G. ruber* in the samples above T2, as contamination should not strongly depend on the foraminiferal species. The strong species dependency of Na/Ca shows that each species gives very specific information on paleo-salinity, depending on ecological variables.

4.3 Size dependency of foraminiferal Na/Ca and Mg/Ca

Culturing studies generally use planktonic foraminifera caught in the water column. These tend to be smaller then those found in the sediment (not all living

foraminifera are fully grown adults). If a size effect on Na/Ca exists, this is problematic. However, Size measurements of foraminifera analyzed with LA-ICP-MS from the Red Sea core KL09 shows no correlation with Na/Ca or Mg/Ca (see figure 3.6). Note that foraminifera smaller than $300\mu m$ were seived out of the samples and therefore not present during analyses. Our data is therefore only applicable to *G. ruber* larger than $300\mu m$.

4.4 Na/Ca as a proxy for salinity

A small sample size does not provide an accurate salinity reconstruction. The inter-individual variability must be know within a sample before conducting solution ICP-MS. This implies that unless the variability is known from another study, solution ICP-MS is not suitable, as it will not be possible to determine how many individuals should be analyzed for an accurate and precise salinity reconstruction. Until such reference curves are available, it is therefore advisable to either use a large number of individuals (> 30) or use LA-ICP-MS instead. Previous salinity reconstructions, such as Wit et al. (2013), use relatively few individuals. While for certain species this may be sufficient, our data suggest that this is certainly not the case for *G. ruber* (white).

In the laser ablation experiments, each chamber (or in some cases, the most possible) is measured individually. The average is then calculated by dividing the sum of all measurements by the amount of measurements. However, the solution ICP-MS essentially measures the weighed average (by mass). This may cause differences between the measurements, as not all chambers are of equal mass and not all chambers have the same composition (see figure 3.7). Furthermore, there could be a size effect on Na/Ca (although not present in our dataset) (Wit et al., 2013) and larger foraminifera tend to be heavier. Consequently, the Na/Ca ratios of larger foraminifera are expected to be over-represented in the solution ICP-MS measurements relative to LA-ICP-MS. The only way to prevent this problem, is by picking foraminifera of the same size. While this has been done to a certain extent, sample size was sometimes insufficient. Moreover, although the average Na/Ca ratios per foram may be calculated from a LA-ICP-MS measured by averaging the measurements of all chambers, the difference in weight between the chambers (which influences the solution ICP-MS measurements) cannot be accounted for. For the reasons stated above, comparing LA-ICP-MS data to solution ICP-MS data is problematic. If enough time is available, LA-ICP-MS should be used. However, if overgrowth and contamination are not present, solution ICP-MS should give the same average per sample. Since solution ICP-MS is much more time efficient compare to LA-ICP-MS when analyzing large amounts of foraminifera, it can still be the best option.

Chapter 5

Conclusion

5.1 Solution ICP-MS versus LA-ICP-MS

Analyses of the core top samples originating from the Mediterranean Sea shows that both LA-ICP-MS and solution ICP-MS can be used to measure the compisition of shells of foraminifera. When comparing these two methods, solution ICP-MS is more time efficient for large sample sets, while LA-ICP-MS allows for studying inter- and intra-individual variance. We also found that either a large salinity gradient or a very large sample set is necessary to detect salinity variability with Na/Ca, due to high inter-individual variance. One of the three core top samples resulted higher Na/Ca with LA-ICP-MS compared to solution ICP-MS, possibly this measurement is an outlier. Alternatively, an error may have been made during second cleaning stage (after LA-ICP-MS, prior to solution ICP-MS).

Inter-individual variability in Na/Ca ratios is very large in our core-top data set, typically $3mmol/mol$ (disregarding outliers). If solution ICP-MS is to be used for Na/Ca measurements, the inter-individual variability of the foraminifera to be measured should be known. This is the only way to determine how many individuals will have to be measured for an accurate and precise result. Furthermore, contaminated foramnifera and individuals with non-biogenic overgrowth should be excluded from analyses. Including such foraminifera may result in non-representative data, as the overgrowth and/or contamination does not necessarily reflect oceanographic conditions during the life of the foraminifer. Overgrowth and contamination can be recognized by inspecting the foraminifera with an electron microscope (see Hoogakker et al. (2009) for examples).

5.2 Red Sea core KL09

LA-ICP-MS data over the interval 146-144 ka shows elevated Mg/Ca, Mn/Ca and Fe/Ca ratios in approximately half of the measurements (see appendix A). It is therefore important to measure each foraminifera individually, as this allows for

outlier removal. Whole batch analyses, such as solution ICP-MS, does not allow for this, as there is only one measurement per sample.

Na/Ca appears to be unaffected by this contamination, as there is no correlation between outliers in Mg/Ca (or any of the other elemental ratios) and Na/Ca in the LA-ICP-MS data (see figure 3.8 and all figure in appendix A). When compared to the Red Sea plankton pump calibration curve (in prep., see figure 3.1), Na/Ca ratio's found in Red Sea core KL09 are too low. Applying this calibration to our data would result in unrealistic salinity values. It is therefore not possible to reconstruct salinity without relying on $\delta^{18}O$ data for reference. Still, current sea level reconstructions based on $\delta^{18}O$ (such as (De Boer et al., 2014)) are of sufficient quality for a qualitative comparison with our dataset. Na/Ca in *G. ruber* shows no correlation with global sea level (figures 3.10 and 3.9). *G. sacculifer* however does show an inverse trend, although the interval is very short. Additional samples over the interval 136-130 ka and from 115 ka onwards are available for measurement. We recommend the measurent of *G. sacculifer* in these samples to either strengthen the relationship between global sea level and Na/Ca or show that the correlation in our data set is coincidental. We conclude that different species can give very different Na/Ca records and that the Na/Ca record of *G. sacculifer* in the Red Sea might be related to salinity, although further research is needed for statistical significance.

Acknowledgment

Firstly, many thanks to my supervisors, Gert-Jan Reichaart and Esmee Geerken for their extensive help with planning, lab work and writing, Wim Boer for his help with the foram cleaning protocol and ICP-MS measurements, Eveline Mezger for sending me her Red Sea calibration curve data, Katherine Grant for providing the samples of core KL09 as well as the associated data and Geert-Jan Brummer for showing me all relevant foraminifera species in the samples, ensuring a swift start. I would like to thank the OCS group for their interest in my study, providing a fresh view on problems encountered. Last but not least I would like to thank everyone in De Potvis, you have been (and still are!) like a family to me.

References

Armstrong, H. and Brasier, M. (2013). *Microfossils*. John Wiley & Sons.

Baker, J., Snee, L., and Menzies, M. (1996). A brief oligocene period of flood volcanism in yemen: implications for the duration and rate of continental flood volcanism at the afro-arabian triple junction. *Earth and Planetary Science Letters*, 138(1):39–55.

Barker, S., Greaves, M., and Elderfield, H. (2003). A study of cleaning procedures used for foraminiferal mg/ca paleothermometry. *Geochemistry, Geophysics, Geosystems*, 4(9).

Cheng, H., Zhang, P., Spötl, C., Edwards, R., Cai, Y., Zhang, D., Sang, W., Tan, M., and An, Z. (2012). The climatic cyclicity in semiarid-arid central asia over the past 500,000 years. *Geophysical Research Letters*, 39(1).

Dansgaard, W. (1964). Stable isotopes in precipitation. *Tellus*, 16(4):436–468.

De Boer, B., Lourens, L. J., and Van De Wal, R. S. (2014). Persistent 400,000-year variability of antarctic ice volume and the carbon cycle is revealed throughout the plio-pleistocene. *Nature communications*, 5.

Elderfield, H. and Ganssen, G. (2000). Past temperature and δ18o of surface ocean waters inferred from foraminiferal mg/ca ratios. *Nature*, 405(6785):442–445.

Ferguson, J., Henderson, G., Kucera, M., and Rickaby, R. (2008). Systematic change of foraminiferal mg/ca ratios across a strong salinity gradient. *Earth and Planetary Science Letters*, 265(1):153–166.

Grant, K., Rohling, E., Ramsey, C. B., Cheng, H., Edwards, R., Florindo, F., Heslop, D., Marra, F., Roberts, A., Tamisiea, M., et al. (2014). Sea-level variability over five glacial cycles. *Nature communications*, 5.

Hays, J. D., Imbrie, J., Shackleton, N. J., et al. (1976). Variations in the earth's orbit: pacemaker of the ice ages. American Association for the Advancement of Science.

Hoogakker, B. A., Klinkhammer, G. P., Elderfield, H., Rohling, E. J., and Hayward, C. (2009). Mg/ca paleothermometry in high salinity environments. *Earth and Planetary Science Letters*, 284(3):583–589.

Imbrie, J., Boyle, E., Clemens, S., Duffy, A., Howard, W., Kukla, G., Kutzbach, J., Martinson, D., McIntyre, A., Mix, A., et al. (1992). On the structure and origin of major glaciation cycles 1. linear responses to milankovitch forcing. *Paleoceanography*, 7(6):701–738.

Laskar, J. (1999). The limits of earth orbital calculations for geological time-scale use. *Philosophical Transactions of the Royal Society of London A: Mathematical, Physical and Engineering Sciences*, 357(1757):1735–1759.

Laskar, J., Fienga, A., Gastineau, M., and Manche, H. (2011a). La2010: a new orbital solution for the long-term motion of the earth. *Astronomy & Astrophysics*, 532:A89.

Laskar, J., Gastineau, M., Delisle, J.-B., Farrés, A., and Fienga, A. (2011b). Strong chaos induced by close encounters with ceres and vesta. *Astronomy & Astrophysics*, 532:L4.

Lisiecki, L. E. and Raymo, M. E. (2005). A pliocene-pleistocene stack of 57 globally distributed benthic δ18o records. *Paleoceanography*, 20(1).

Millot, C. and Taupier-Letage, I. (2005). Circulation in the mediterranean sea. In *The Mediterranean Sea*, pages 29–66. Springer.

Rohling, E., Sprovieri, M., Cane, T., Casford, J., Cooke, S., Bouloubassi, I., Emeis, K., Schiebel, R., Rogerson, M., Hayes, A., et al. (2004). Reconstructing past planktic foraminiferal habitats using stable isotope data: a case history for mediterranean sapropel s5. *Marine Micropaleontology*, 50(1):89–123.

Rohling, E. J. and Bigg, G. R. (1998). Paleosalinity and 5180: A critical assessment. *J. Geophys. Res*, 103:1307–1318.

Rohling, E. J., Grant, K., Hemleben, C., Siddall, M., Hoogakker, B., Bolshaw, M., and Kucera, M. (2008). High rates of sea-level rise during the last interglacial period. *Nature Geoscience*, 1(1):38–42.

Rosenthal, Y., Lohmann, G., Lohmann, K., and Sherrell, R. (2000). Incorporation and preservation of mg in globigerinoides sacculifer: Implications for reconstructing the temperature and 18o/16o of seawater. *Paleoceanography*, 15(1):135–145.

Siddall, M., Smeed, D. A., Hemleben, C., Rohling, E. J., Schmelzer, I., and Peltier, W. R. (2004). Understanding the red sea response to sea level. *Earth and Planetary Science Letters*, 225(3):421–434.

Trommer, G., Siccha, M., Rohling, E., Grant, K., Van der Meer, M., Schouten, S., Baranowski, U., and Kucera, M. (2011). Sensitivity of red sea circulation to sea level and insolation forcing during the last interglacial. *Climate of the Past*, 7(3):941–955.

Vidal, E., Pascual, A., Barnier, B., Molines, J.-M., and Tintoré, J. (2011). Analysis of a 44-year hindcast for the mediterranean sea: comparison with altimetry and in situ observations. *Scientia Marina*, 75(1):71–86.

Wang, L. (2000). Isotopic signals in two morphotypes of globigerinoides ruber (white) from the south china sea: implications for monsoon climate change during the last glacial cycle. *Palaeogeography, Palaeoclimatology, Palaeoecology*, 161(3):381–394.

Wit, J. C., de Nooijer, L., Wolthers, M., and Reichart, G.-J. (2013). A novel salinity proxy based on na incorporation into foraminiferal calcite.

Zachos, J., Pagani, M., Sloan, L., Thomas, E., and Billups, K. (2001). Trends, rhythms, and aberrations in global climate 65 ma to present. *Science*, 292(5517):686–693.

Appendix A

XY plots prior to filtering

Negative and extremely high (¿1000mmol/mol) ratio's are not shown.

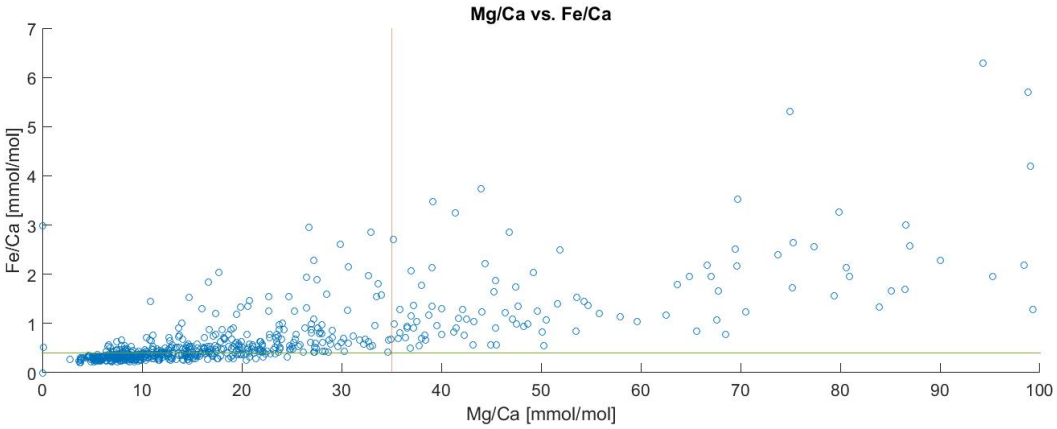

Figure A.1: Mg/Ca versus Fe/Ca of the unfiltered KL09 LA data. The solid lines indicate the upper limit of each element.

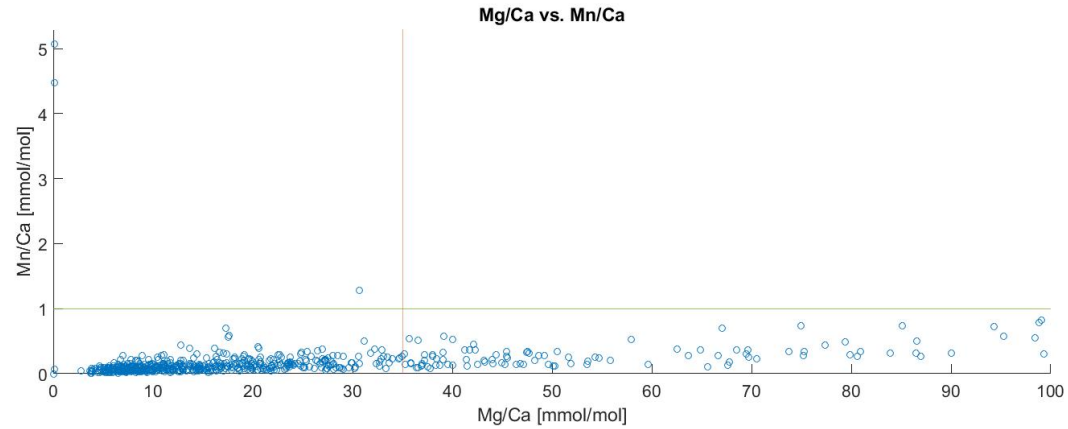

Figure A.2: Mg/Ca versus Mn/Ca of the unfiltered KL09 LA data. The solid lines indicate the upper limit of each element.

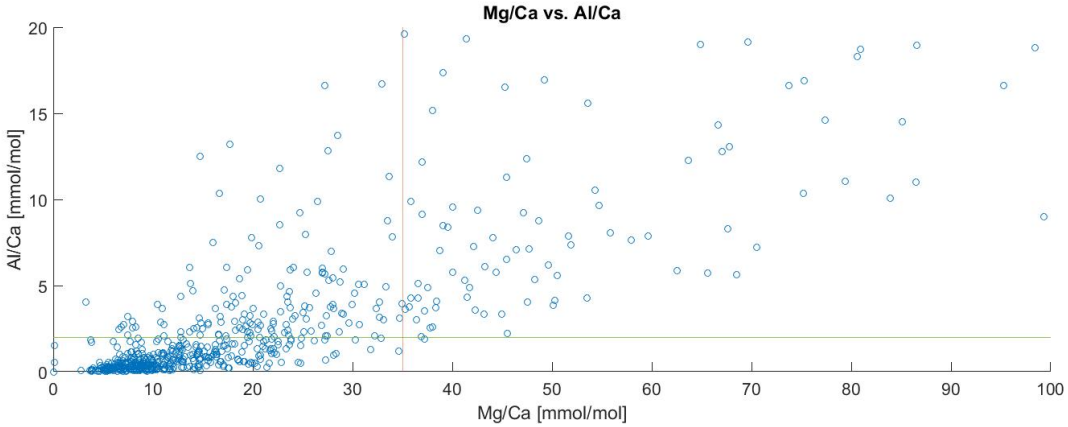

Figure A.3: Mg/Ca versus Al/Ca of the unfiltered KL09 LA data. The solid lines indicate the upper limit of each element.

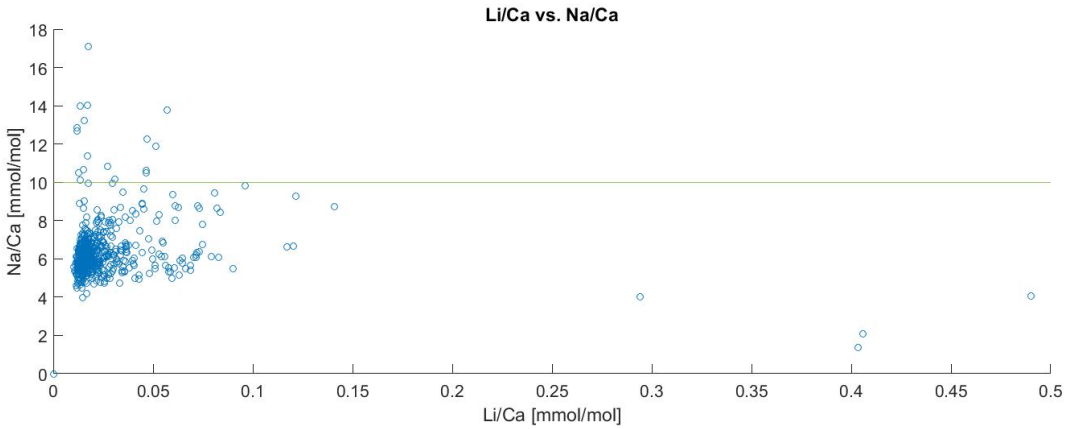

Figure A.4: Li/Ca versus Na/Ca of the unfiltered KL09 LA data. The solid lines indicate the upper limit of each element.

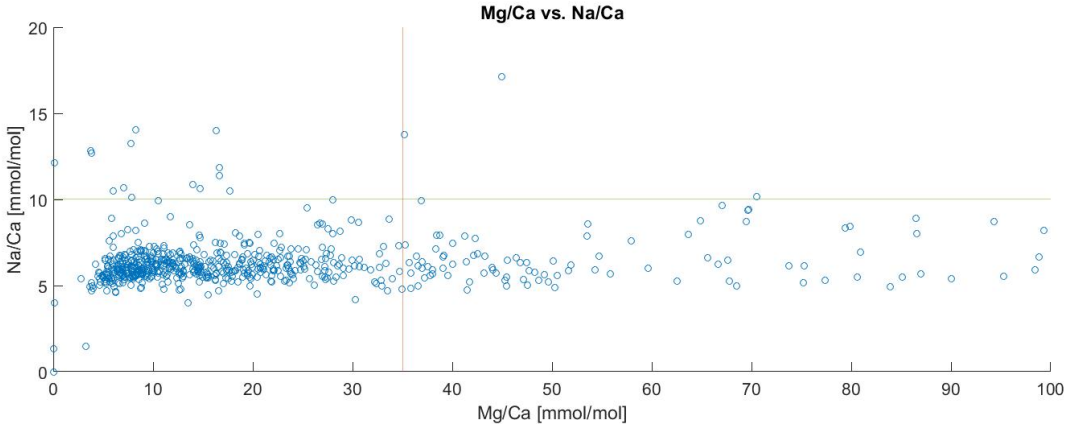

Figure A.5: Mg/Ca versus Na/Ca of the unfiltered KL09 LA data. The solid lines indicate the upper limit of each element.

Appendix B

Appendix: Matlab scripts

In this section the matlab scripts are presented. Note that not all figures are used in the final version of this thesis. Furthermore, some figures have been edited using the figure property editor after running the script.

B.1 KL09LA

```
%In this script, LA data from KL09 (red sea) is processed. the required
%input per sample is age, Mg/Ca (label as MgCa),Na/Ca (label as NaCa) and
%sample number (label as sample). Furthermore, the age per sample has to
%defined in a seperate vector.

close all
load KL09LAdata.mat
load KL09LAdataunfiltered
%% input

for i=[110 120 121 122 123 125 126 127 128 129 130 131]; %index number of
NaCapsz(i)=mean(NaCa(find(sample==i)));
NaCapsstdz(i)=std(NaCa(find(sample==i)))/sqrt(length(NaCa(find(sample==i)
MgCapsz(i)=mean(MgCa(find(sample==i)));
MgCapsstdz(i)=std(MgCa(find(sample==i)))/sqrt(length(MgCa(find(sample==i)
sizepsz(i)=mean(size(find(sample==i)));
end
NaCaps=NaCapsz(find(NaCapsz>0));
NaCapsstd=NaCapsstdz(find(NaCapsstdz>0));
MgCapsstd=MgCapsstdz(find(MgCapsstdz>0));
MgCaps=MgCapsz(find(MgCapsz>0));
sizeps=sizepsz(find(sizepsz>0));

sizepsstd(1)=3*std(size(find(sample==110)))/sqrt(length(size(find(sample=
```

```
sizepsstd(2)=3*std(size(find(sample==120)))/sqrt(length(size(find(sample=
sizepsstd(3)=3*std(size(find(sample==121))/sqrt(length(size(find(sample==
sizepsstd(4)=3*std(size(find(sample==122)))/sqrt(length(size(find(sample=
sizepsstd(5)=3*std(size(find(sample==123)))/sqrt(length(size(find(sample=
sizepsstd(6)=3*std(size(find(sample==125)))/sqrt(length(size(find(sample=
sizepsstd(7)=3*std(size(find(sample==126)))/sqrt(length(size(find(sample=
sizepsstd(8)=3*std(size(find(sample==127)))/sqrt(length(size(find(sample=
sizepsstd(9)=3*std(size(find(sample==128)))/sqrt(length(size(find(sample=
sizepsstd(10)=3*std(size(find(sample==129)))/sqrt(length(size(find(sample
sizepsstd(11)=3*std(size(find(sample==130)))/sqrt(length(size(find(sample
sizepsstd(12)=3*std(size(find(sample==131)))/sqrt(length(size(find(sample

ageps=([143.96262 145.2668 145.4054 145.544 145.6825 145.9595 146.098 146
]); %A list of the age of each sample, has to be in the same order as the

%here, the chambers are seperated, for all
%samples
NaCach1=NaCa(find(chamber==1));
NaCach2=NaCa(find(chamber==2));
NaCach3=NaCa(find(chamber==3));
MgCach1=MgCa(find(chamber==1));
MgCach2=MgCa(find(chamber==2));
MgCach3=MgCa(find(chamber==3));
sizech1=size(find(chamber==1));
sizech2=size(find(chamber==2));
sizech3=size(find(chamber==3));
FeCach1=FeCa(find(chamber==1));
FeCach2=FeCa(find(chamber==2));
FeCach3=FeCa(find(chamber==3));
MnCach1=FeCa(find(chamber==1));
MnCach2=FeCa(find(chamber==2));
MnCach3=FeCa(find(chamber==3));
AlCach1=FeCa(find(chamber==1));
AlCach2=FeCa(find(chamber==2));
AlCach3=FeCa(find(chamber==3));

for i=1:3 %standard error per chamber, for all samples
NaCapc(i)=mean(NaCa(find(chamber==i)));
NaCapcstd(i)=std(NaCa(find(chamber==i)))/sqrt(length(find(chamber==i)));
MgCapc(i)=mean(MgCa(find(chamber==i)));
MgCapcstd(i)=std(MgCa(find(chamber==i)))/sqrt(length(find(chamber==i)));
FeCapc(i)=mean(FeCa(find(chamber==i)));
FeCapcstd(i)=std(FeCapc(i))/sqrt(length(find(chamber==i)));
MnCapc(i)=mean(MnCa(find(chamber==i)));
```

```
MnCapcstd(i)=std(MnCapc(i))/sqrt(length(find(chamber==i)));
AlCapc(i)=mean(AlCa(find(chamber==i)));
AlCapcstd(i)=std(AlCapc(i))/sqrt(length(find(chamber==i)));
end
chamberpc=[1 2 3]; %chamber per chamber always results in a single value
%% figures
subplot(3,1,1)
errorbar(ageps,NaCaps,NaCapsstd)
axis([143.5 147 5 8])
xlabel('age [kyr]')
ylabel('Na/Ca [mmol/mol]')
set(gca,'color','none') ;

subplot(3,1,2)
errorbar(ageps,MgCaps,MgCapsstd)
xlabel('age [kyr]')
ylabel('Mg/Ca [mmol/mol]')
set(gca,'color','none') ;

subplot(3,1,3)
errorbar(ageps,sizeps,sizepsstd)
xlabel('age [kyr]')
ylabel('size [um]')
set(gca,'color','none') ;

figure
subplot(1,2,1)
hist(MgCa)
xlabel('Mg/Ca [mmol/mol]')
ylabel('amount [-]')
subplot(1,2,2)
hist(NaCa)
xlabel('Na/Ca [mmol/mol]')
ylabel('amount [-]')

figure
subplot(1,2,1)
scatter(size,NaCa,'+')
ylabel('Na/Ca [mmol/mol]')
xlabel('size [um]')
subplot(1,2,2)
scatter(size,MgCa,'+')
ylabel('Mg/Ca [mmol/mol]')
xlabel('size')
```

```
figure
plot(NaCach1,MgCach1,'+',NaCach2,MgCach2,'or',NaCach3,MgCach3,'ob')
xlabel('Na/Ca [mmol/mol]')
ylabel('Mg/Ca [mmol/mol]')
legend('chamber 1','chamber 2','chamber 3')

figure
subplot(1,2,1)
errorbar(chamberpc,NaCapc,NaCapcstd,'.','markers',20)
xlabel('chamber')
ylabel('Na/Ca [mmol/mol]')
ax = gca;
ax.XTick = [1 2 3];
ax.XTickLabel = {'F-2','F-1','F'};

subplot(1,2,2)
errorbar(chamberpc,MgCapc,MgCapcstd,'.','markers',20)
xlabel('chamber')
ylabel('Mg/Ca [mmol/mol]')
ax = gca;
ax.XTick = [1 2 3];
ax.XTickLabel = {'F-2','F-1','F'};

% subplot(1,5,3)
% errorbar(chamberpc,FeCapc,FeCapcstd,'.','markers',20)
% xlabel('chamber')
% ylabel('Fe/Ca [mmol/mol]')
% ax = gca;
% ax.XTick = [1 2 3];
% ax.XTickLabel = {'F-2','F-1','F'};
%
% subplot(1,5,4)
% errorbar(chamberpc,MnCapc,MnCapcstd,'.','markers',20)
% xlabel('chamber')
% ylabel('Mn/Ca [mmol/mol]')
% ax = gca;
% ax.XTick = [1 2 3];
% ax.XTickLabel = {'F-2','F-1','F'};
%
% subplot(1,5,5)
% errorbar(chamberpc,AlCapc,AlCapcstd,'.','markers',20)
% xlabel('chamber')
% ylabel('Al/Ca [mmol/mol]')
```

```
% ax = gca;
% ax.XTick = [1 2 3];
% ax.XTickLabel = {'F-2','F-1','F'};
%
%% plot met d180 en na voor alle data, ook solution
figure
subplot(3,1,1)
%d18O
h = plot(x8, y8,'*',a,yfit_8,'--k');
legend( h, 'd18O', 'linear interpolation','Fit', 'Location', 'NorthEast'
grid on
axis([110 145 -3.6 2.2])
ylabel ('d18O (promille)')
set(gca,'color','none') ;

%Na/Ca
x=115:0.001:129.3;
a=88:0.001:145;
figure
subplot(3,1,1)
hold on
h = plot(x1, y1,'.b', x3, y3,'.r',...
    x,yfit_1,'--b', x,yfit_3,'--r');
legend( h, 'Na/Ca ruber', 'Na/Ca sacculifer', 'Location', 'NorthEast' );
ylabel ('Na/Ca [mmol/mol]')
errorbar(x1,y1,y1*0.02,'--k')
errorbar(x3,y3,y3*0.02,'--k')
errorbar(ageps,NaCaps,NaCapsstd)
grid off
axis([100 200 4 8])
hold off
set(gca,'color','none') ;
set(gca,'Ydir','reverse')
subplot(3,1,3)
xlabel('age [kyr]')
ylabel('Na/Ca [mmol/mol]')

plot(-age_calkaBP,sealev)
legend('Sea level')
axis([100 200 -120 20])
grid off;
set(gca,'color','none');
xlabel('age [kyr]')
ylabel('Global sea level [m]')
```

```
subplot(3,1,2)
plot(x6,y6,'oR',x,yfit_6,'--R')
grid off
axis([100 200 0 50])
set(gca,'color','none') ;
xlabel('age [kyr]')
ylabel('Mg/Ca [mmol/mol]')
%% XY plots prior to filtering
figure
scatter(unfilteredmat(:,4),unfilteredmat(:,6)) %Li/Ca vs. Na/Ca
hold on
plot(unfilteredmat(:,4),10*ones(length(unfilteredmat(:,7))));
hold off
title('Li/Ca vs. Na/Ca')
axis([0 0.5 0 18])
xlabel('Li/Ca [mmol/mol]')
ylabel('Na/Ca [mmol/mol]')

figure
scatter(unfilteredmat(:,7),unfilteredmat(:,6)) %Mg/Ca vs. Na/Ca
axis([0 100 0 20])
hold on
plot(unfilteredmat(:,7),10*ones(length(unfilteredmat(:,7))));
plot(35*ones(length(unfilteredmat(:,7))),unfilteredmat(:,7));
hold off
title('Mg/Ca vs. Na/Ca')
ylabel('Na/Ca [mmol/mol]')
xlabel('Mg/Ca [mmol/mol]')

figure
scatter(unfilteredmat(:,7),unfilteredmat(:,9)) %Mg/Ca vs. Al/Ca
hold on
plot(unfilteredmat(:,7),2*ones(length(unfilteredmat(:,7))));
plot(35*ones(length(unfilteredmat(:,7))),unfilteredmat(:,7));
hold off
axis([0 100 0 20])
title('Mg/Ca vs. Al/Ca')
ylabel('Al/Ca [mmol/mol]')
xlabel('Mg/Ca [mmol/mol]')

figure
scatter(unfilteredmat(:,7),unfilteredmat(:,13)) %Mg/Ca vs. Fe/Ca
hold on
```

```
plot(unfilteredmat(:,7),ones(length(unfilteredmat(:,7))));
plot(35*ones(length(unfilteredmat(:,7))),unfilteredmat(:,7));
hold off
axis([0 100 0 8])
title('Mg/Ca vs. Mn/Ca')
ylabel('Mn/Ca [mmol/mol]')
xlabel('Mg/Ca [mmol/mol]')

figure
scatter(unfilteredmat(:,7),unfilteredmat(:,14)) %Mg/Ca vs. Mn/Ca
hold on
plot(unfilteredmat(:,7),0.4*ones(length(unfilteredmat(:,7))));
plot(35*ones(length(unfilteredmat(:,7))),unfilteredmat(:,7));
hold off
axis([0 100 0 10])
title('Mg/Ca vs. Fe/Ca')
ylabel('Fe/Ca [mmol/mol]')
xlabel('Mg/Ca [mmol/mol]')
%% XY plots na filteren
figure
subplot(2,2,1)
scatter(MgCa,NaCa)
ylabel('Na/Ca [mmol/mol]')
xlabel('Mg/Ca [mmol/mol]')
subplot(2,2,2)
scatter(MgCa,MnCa)
ylabel('Fe/Ca [mmol/mol]')
xlabel('Mg/Ca [mmol/mol]')
subplot(2,2,3)
scatter(MgCa,FeCa)
ylabel('Fe/Ca [mmol/mol]')
xlabel('Mg/Ca [mmol/mol]')
subplot(2,2,4)
scatter(MgCa,AlCa)
ylabel('Al/Ca [mmol/mol]')
xlabel('Mg/Ca [mmol/mol]')
```

B.2 KL09

```
%in this script, all data from core KL09 is processed
clc
```

```
close all %this command closes all open matlab figures
load KL09data.mat
set(0,'DefaultLineMarkerSize',10);

%% input arguments
rwindex=(find(species==1));
sacindex=(find(species==2));
NaCarw=Na23Ca43_BLK(rwindex);
NaCasac=Na23Ca43_BLK(sacindex);
MgCarw=MgCa_BLK(rwindex);
MgCasac=MgCa_BLK(sacindex);
agerw=age(rwindex);
agesac=age(sacindex);
AlCasac=Al27Ca43_BLK_corr(sacindex);
KCasac=K39Ca43_BLK_corr(sacindex);
MnCasac=Mn55Ca43_BLK_corr(sacindex)*(0.084/0.21);
AlCarw=Al27Ca43_BLK_corr(rwindex);
KCarw=K39Ca43_BLK_corr(rwindex);
MnCarw=Mn55Ca43_BLK_corr(rwindex)*(0.084/0.21);

[fitresult1, ~,x1,y1] = nacarw_PD2(agerw, NaCarw);
[fitresult2, ~,x2,y2] = mgcarwfit_PD(agerw, MgCarw);
[fitresult3, ~,x3,y3] = nacafitsac_PD(agesac, NaCasac);
[fitresult4, ~,x4,y4] = mncarwfit_PD(agerw, MnCarw);
[fitresult5, ~,x5,y5] = mncasacfit_PD(agesac, MnCasac);
[fitresult6, ~,x6,y6] = mgcasacfit_PD(agesac, MgCasac);
[fitresult7, ~,x7,y7] = d18O_PD(agesi, d18O);
[fitresult8, ~,x8,y8] = d18Ofitlang_PD(agelang, d18Olang);

x=115:0.001:129.3;
a=88:0.001:145;
yfit_1=fitresult1(x);
yfit_2=fitresult2(x);
yfit_3=fitresult3(x);
yfit_4=fitresult4(x);
yfit_5=fitresult5(x);
yfit_6=fitresult6(x);
yfit_7=fitresult7(x);
yfit_8=fitresult8(a);


%% d18O, d13C, katherines measurements, uncomment to plot
% figure
% subplot(2,1,1)
```

```
% scatter(agesi,d18O)
% xlabel('age [kyr]')
% ylabel('d18O vPDB (promille)')
% grid minor
% subplot(2,1,2)
% scatter(agesi,d13C)
% xlabel('age [kyr]')
% ylabel('d13C vPDB (promille)')
% grid minor


%% Na/Ca, Mg/Ca, uncomment to plot
% figure
% subplot(2,1,1)
% hold on
% scatter(agesac,NaCasac)
% scatter(agerw,NaCarw,'^')
% hold off
% ylabel('Na/Ca [mmol/mol')
%
% legend('G. sacculifer','G. ruber')
% set(gca,'XTick',[])
% set(gca,'XColor','w')
% grid minor
%
% subplot(2,1,2)
% hold on
% scatter(agesac,MgCasac)
% scatter(agerw,MgCarw,'^')
% hold off
% xlabel('Age [kyr]')
% ylabel('Mg/Ca [mmol/mol')
% legend('G. sacculifer','G. ruber')
% grid minor
% axis ([113 130 6 20])


%% other elements, uncomment to plot
% figure
% subplot(2,3,1)
% scatter(agesac,AlCasac)
% title('G. sacculifer, Al/Ca')
% xlabel('Age [kyr]')
% ylabel('Al/Ca [mmol/mol')
```

```
% grid minor
% axis([115 130 0 2*10^(-4)])
%
% subplot(2,3,2)
% scatter(agesac,KCasac)
% title('G. sacculifer, K/Ca')
% xlabel('Age [kyr]')
% ylabel('K/Ca [mmol/mol')
% grid minor
%
% subplot(2,3,3)
% scatter(agesac,MnCasac)
% title('G. sacculifer, Mn/Ca')
% xlabel('Age [kyr]')
% ylabel('Mn/Ca [mmol/mol')
% grid minor
% axis([115 130 0 0.7])
%
% subplot(2,3,4)
% scatter(agerw,AlCarw)
% title('G. ruber, Al/Ca')
% xlabel('Age [kyr]')
% ylabel('Al/Ca [mmol/mol')
% grid minor
% axis([115 130 0 2*10^(-4)])
%
% subplot(2,3,5)
% scatter(agerw,KCarw)
% title('G. ruber, K/Ca')
% xlabel('Age [kyr]')
% ylabel('K/Ca [mmol/mol')
% grid minor
% axis([115 130 0 0.7])
%
% subplot(2,3,6)
% scatter(agerw,MnCarw)
% title('G. ruber, Mn/Ca')
% xlabel('Age [kyr]')
% ylabel('Mn/Ca [mmol/mol')
% grid minor
% axis([115 130 0 0.7])
%% All interpolations , uncomment to plot
figure
h = plot(x1, y1,'ob', x2, y2,'sr',...
```

```
    x,yfit_1,'--k', x,yfit_2,'--k');
legend( h, 'Na/Ca ruber', 'Mg/Ca ruber','Fit', 'Location', 'NorthEast' );
axis([117 129.5 5 20])


figure
h = plot(x1, y1,'ob', x4, y4,'sr',...
    x,yfit_1,'--k', x,yfit_4,'--k');
legend( h, 'Na/Ca ruber', 'Mn/Ca ruber','Fit', 'Location', 'NorthEast' );

figure
h = plot(x1, y1,'ob', x3, y3,'sr',...
    x,yfit_1,'--b', x,yfit_3,'--r',...
x,yfit_1*1.02,'--b',x,yfit_1*0.98,'--b', x,yfit_3*1.02,'--r', x,yfit_3*0.
legend( h, 'Na/Ca ruber', 'Na/Ca sacculifer','Interpolation, shape preser
axis([115,129.5,4.5,7.5])
ylabel ('Na/Ca [mmol/mol]')
xlabel ('age [kyr]')

grid on
figure
subplot(2,3,1)
scatter(x1,y1)
ylabel 'Na/Ca ruber'
xlabel 'age [kyr]'
subplot(2,3,2)
scatter(x2,y2)
ylabel 'Mg/Ca ruber'
xlabel 'age [kyr]'
subplot(2,3,3)
scatter(x4,y4)
ylabel 'Mn/Ca ruber'
xlabel 'age [kyr]'
subplot(2,3,4)
scatter(x3,y3)
ylabel 'Na/Ca sacculifer'
xlabel 'age [kyr]'
subplot(2,3,5)
scatter(x6,y6)
ylabel 'Mg/Ca sacculifer'
xlabel 'age [kyr]'
subplot(2,3,6)
scatter(x5,y5)
ylabel 'Mn/Ca sacculifer'
```

```
xlabel 'age [kyr]'

figure
hold on
[Ax,p1,p2]=plotyy(x,yfit_1,x,yfit_2);
plot(x,yfit_3,'b');
legend('Na/Ca ruber','Na/Ca sacculifer','mg/Ca ruber')
xlabel('age [kyr]');
ylabel((Ax(1)),'Na/Ca [mmol/mol]');
ylabel((Ax(2)),'Mg/Ca [mmol/mol]');

figure
h = plot(x2, y2,'ob', x6, y6,'sr',...
    x,yfit_2,'--b', x,yfit_6,'--r',...
    x,yfit_2*1.04,'--b',x,yfit_2*0.96,'--b', x,yfit_6*1.04,'--r', x,yfit_
legend( h, 'Mg/Ca ruber', 'Mg/Ca sacculifer','Interpolation, shape preser
axis([114 129.5 5 44])
ylabel 'Mg/Ca [mmol/mol]'
xlabel 'age [kyr]'
grid on
%% XY plots

figure
h=plot(y3,y5,'or',y1,y4,'ob');
axis([5 6.4 0 0.3])
legend('Na/Ca (sacculifer) vs. Mn/Ca (sacculifer)','Na/Ca (ruber) vs. Mn/
xlabel('Na/Ca [mmol/mol]')
ylabel('Mn/Ca [mmol/mol]')
grid  on
%% plot met d18O en na,mg,mn
figure
subplot(3,1,1)
%d18O
h = plot(x8, y8,'*',a,yfit_8,'--k');
legend( h, 'd18O', 'linear interpolation','Fit', 'Location', 'NorthEast'
grid on
axis([110 145 -3.6 2.2])
ylabel ('d18O (promille)')
set(gca,'color','none') ;

%Na/Ca
subplot(3,1,2)
hold on
h = plot(x1, y1,'.b', x3, y3,'.r',...
```

```
    x,yfit_1,'--b', x,yfit_3,'--r');
legend( h, 'Na/Ca ruber', 'Na/Ca sacculifer', 'Location', 'NorthEast' );
ylabel ('Na/Ca [mmol/mol]')
errorbar(x1,y1,y1*0.02,'--k')
errorbar(x3,y3,y3*0.02,'--k')
grid on
axis([110 145 5 7.5])
hold off
set(gca,'color','none') ;

%Mg/Ca
subplot(3,1,3)
hold on
h = plot(x2, y2,'.b', x6, y6,'.r',...
    x,yfit_2,'--b', x,yfit_6,'--r');
legend( h, 'Mg/Ca ruber', 'Mg/Ca sacculifer', 'Location', 'NorthEast' );
axis([115,129.5,4.5,7.5])
ylabel ('Mg/Ca [mmol/mol]')
xlabel ('age [kyr]')
errorbar(x2,y2,y2*0.04,'--k')
errorbar(x6,y6,y6*0.04,'--k')
grid on
axis([110 145 6 44])
set(gca,'color','none') ;
hold off
```

B.3 Maps

```
% A script to plot the  Mediterranean Sea including the measuring sites
% pieter Dirksen, March 2016
% ------------------------------------------------------------------------

clear all; close all
%KL09:  0.381050000 19.9600000
coord=[%38.105 19.96,
    15 33,
    20 37,
    12 40,
    7 43];

hold on
plot(coord(1,1),coord(1,2),'o','MarkerEdgeColor','k','MarkerFaceColor','k
```

```
plot(coord(2,1),coord(2,2),'d','MarkerEdgeColor','k','MarkerFaceColor','r
plot(coord(3,1),coord(3,2),'v','MarkerEdgeColor','k','MarkerFaceColor','y
plot(coord(4,1),coord(4,2),'h','MarkerEdgeColor','k','MarkerFaceColor','c

legend('punt 1','Punt 2','Punt 3','Punt 4')
%axis([32 45 10 30]) %rode zee
axis([-10 40 30 45]) %middelandse zee
xlabel('Longitude [deg]')
ylabel('Lattitude [deg]')
title('Measurement spots')

% the Natural earth files:
filename='ne_10m_admin_0_countries_lakes.shp'
direct='C:\Users\User\Dropbox\Pieter\';
[S,A] = shaperead([direct filename]);
plot([S.X],[S.Y],'-k')

% C=parula(19);c_offset=4;
C=gray(19);c_offset=4;
D=0.5*ones(19,3);
for k=1:length(A)
country_color=D(A(k).mapcolor9+c_offset,:);
lon=[S(k).X];lat=[S(k).Y];
m=find(isnan(lon)==1);
hold on
fill(lon(1:m(1)-1),lat(1:m(1)-1),country_color);
for n=1:length(m)-1
 fill(lon(m(n)+1:m(n+1)-1),lat(m(n)+1:m(n+1)-1),country_color)
end
end

hold off
```